2015

Thermal transport in DNA

Zaoli Xu
Iowa State University

Thermal transport in DNA

by

Zaoli Xu

A dissertation submitted to the graduate faculty

in partial fulfillment of the requirements for the degree of

DOCTOR OF PHILOSOPHY

Major: Mechanical Engineering

Program of Study Committee:
Xinwei Wang, Major Professor
Daniel Attinger
Gap-Yong Kim
Reza Montazami
Chenxu Yu

Iowa State University

Ames, Iowa

2015

TABLE OF CONTENTS

LIST OF FIGURES

LIST OF TABLES

ACKNOWLEDGEMENTS

First and foremost, I want to thank my major professor Dr. Xinwei Wang for his support in the past four years. Many times I am enlightened by his professional insights and technical advice when I get stuck on my project. Without his guidance, the work could not have been accomplished.

I would also like to thank the other members serving on my POS committee: Dr. Chenxu Yu, Dr. Reza Montazami, Dr. Daniel Attinger, and Dr. Gap-Yong Kim for providing me with all the valuable inputs for my research.

I also want to thank my colleagues who I have worked with in the Micro/Nanoscale Thermal Science Laboratory, former and present: Shen Xu, Chong Li, Jing Liu, Chris Reilly, Zhe Cheng, Yangsu Xie, Jingchao Zhang, Xiaoduan Tang, Guoqing Liu, Nathan Van Velson, Xuhui Feng, Xiaopeng Huang, Yanan Yue, Xiangwen Chen, Huan Lin, Pengyu Yuan, Meng Han, Bowen Zhu, and Tianyu Wang. I wish the best of luck to all of them in their future.

I would also like to express my deepest gratitude to my family, especially my parents Taiyou Xu and Tao Zhang, for their unconditional love, support, and encouragement. Last but not least, I want to thank all my friends in Ames, especially all the soccer teammates in Midfielder. The joyful time we have spent together refreshes me to carry on my research work.

ABSTRACT

Thermal transport in DNA is systematically studied to facilitate the development of DNA-based nanoelectronics in thermal management aspect. Synthesis of crystalline DNA-composited microfiber and microfilm, DNA nanofiber and DNA nanofiber array are developed in sequence to enable the thermal transport study in them. Thermo-physical properties, including thermal conductivity, thermal diffusivity, and volumetric heat capacity, for all of the DNA samples are reported. The thermal conductivity of DNA microfiber is evaluated to be 0.33 W/m·K at room temperature. With the formation of crystalline DNA-NaCl complexes, DNA molecules are speculated to be aligned with the crystal structure of NaCl during crystallization, which results in a significant enhancement of thermal transport. The thermal conduction can also be improved by eliminating structural defects in DNA samples based on the newly-established thermal reffusivity theory. Thermal reffusivity is the inverse of thermal diffusivity and is introduced to quantitatively evaluate phonon scattering induced by structural defects. The structural size for defect-induced phonon scattering is determined to be 0.8 nm for DNA microfiber, in the same order of magnitude as the characteristic size of DNA. As the structural size for defect-induced phonon scattering approaches infinity, the thermal transport potential in defect-free material can be reached. By estimation, the thermal conductivity/diffusivity will be promoted by 36~61% without structural defects in DNA microfiber. Compared to microfiber, DNA nanofiber possesses a higher thermal conductivity due to more condensed and oriented structures, as well as less structural defects. The structural size for defect-induced phonon scattering is 1.6 nm in DNA nanofiber, twice of that in DNA microfiber. The thermal conductivity of DNA nanofiber with perfect structure is predicted to reach 2.3 W/m·K. In addition, nanoscale Ir thin film on DNA microfiber shows a similar intrinsic electrical resistivity

as bulk Ir, which is proposed to be preserved by coherent quantum tunneling and diffusive thermal hopping for electron transport in DNA.

CHAPTER 1. INTRODUCTION

1.1. DNA: engineering material

Deoxyribonucleic acid (DNA) plays a vital role as the carrier of biological information for its base sequences. The genetic alphabet of DNA is formed with four bases, which are guanine (G), cytosine(C), adenine (A) and thymine (T). A G base pairs with a C base, while an A base pairs with a T base. The base-pairing rule defines the genetic codes in all creatures. As a matter of fact, DNA has also been seen as a promising molecular engineering material because of the sequence-specific molecular recognition and self-assembly capabilities to construct nanostructures, including nanoaggregates,[1] nanocrystals,[2] nanowires,[3] and especially functional structures for nanoelectronics.[4] The bottom-up nanofabrication technique may be capable of overcoming the limitations in current scaling down technology for transistor size. In the past few decades, the electronics industry has been driven by the continued scaling down of lithographic transistor size. The scaling allows more transistors to be integrated on a single chip and thus provides greater functionality. Unfortunately, the size of typical half-pitch (half the spacing between identical components) on a chip is getting difficult to go below 22 nm by using the standard complementary-metal-oxide-semiconductor (CMOS) technologies. Scaling down to 14 nm or smaller is possible but the process has been slowed down. Further scaling down may be also no longer reliable and cost effective. Alternatively, the bottom-up nanofabrication with DNA could easily overcome the limits and lead to a whole new way of looking at scaling. More particularly, DNA offers specificity with the base sequences so that the architectural structure of DNA-based nanoelectronics could be highly controlled.

1.2. Electrical conduction in DNA

In order to explore the potential applications in nanoelectronics, the electrical properties of DNA have been extensively studied. Studies illustrate that the electrical properties of DNA are versatile.[5] The charge transport along a DNA molecule over a few nanometers has been explained by several mechanisms, including two dominant processes: coherent quantum tunneling and diffusive thermal hopping.[6-8] A hole, i.e. a positive charge, is more stable on a G-C base pair than on an A-T base pair,[5] thus the A-T base pairs act as the barrier to hole transfer. Coherent quantum tunneling consists of a single-step tunneling process from the first G-C site to the second. The rate of such reaction decays exponentially with the distance. Diffusive thermal hopping, the second mechanism, is a multi-step process between two G-C base pairs. Such hopping process can transfer charge over far longer distance than the coherent quantum tunneling. By contrast, long-range (>50 nm) charge transport measurements along DNA have obtained a range of seemingly contradictory results. Some report that DNA is a semiconductor or an insulator,[9-13] while others reveal that DNA is intrinsically conductive[14-15] or even superconductive.[16] As a consequence, the electrical conductivity of long DNA chain is believed to depend on its length, base sequences and ambient conditions.

1.3. Thermal conduction in DNA

Though the thermal management is also crucial in designing DNA-based nanoelectronics, thermal conduction in DNA still remains largely unexplored. Only a few studies on the thermal transport in DNA have been reported. Simulation results suggest that

DNA is a poor heat conductor with low thermal conductivity. Peyrard-Bishop-Dauxois (PBD) model predicts that the thermal conductivity of DNA is 1.8×10^{-3} W/m·K at 300 K,[17] and a 3-D coarse-grained model estimates that the thermal conductivity of a homogeneous polyG-polyC DNA is 0.3 W/m·K and nonhomogeneous DNA is even lower.[18] The only available experimental result is from the measurement carried out on a DNA-gold composite.[19] The measurement shows a thermal conductivity of 150 W/m·K for the composite, orders of magnitude higher than the simulation results. In the composite, the overall thermal conductivity of the composite can be expressed as $k_s = k_{DNA}(1-\chi)+k_{Au}\chi$, where $\chi = 98.2\%$ is the ratio of cross sectional area for gold coating. The thermal conductivity of gold coating k_{Au} is estimated to be in the order of 100 W/m·K, which indicates that the gold coating dominates the thermal transport in the composite. Whatever the thermal conductivity of DNA is, its contribution to the thermal transport is small due to the small ratio of cross sectional area for DNA. As a consequence, the thermal conductivity of DNA has not yet been determined experimentally.

The understanding of thermal transport in DNA is also vital to decode DNA denaturation via thermal fluctuations.[17] The double-stranded DNA can unravel into two single strands and denaturate, which is important for its relationship to DNA transcription. Denaturation usually occurs when DNA is subjected to elevated temperature or to extreme ionic concentration. The temperature at which half of the DNA strands are in the random coil or in single-stranded state is defined as melting temperature. However, local melting of DNA via thermal fluctuations can occur well below the melting temperature, which is thought to play a major role in the formation of transcription bubble.[20] The detailed information on the

dynamics of the thermal fluctuations and their interaction along the strands are encoded in the thermal transport. Thermal conduction property of DNA is shown to change significantly as it denatures.[17] Thus, the alteration of thermal conduction property is able to probe DNA denaturation via thermal fluctuation. However, the modeling results have contrary conclusions on the alteration of thermal conductance of DNA upon denaturation. The PBD model predicts a substantial increase in the thermal conductance, while another nonlinear model shows a drop in the thermal conductance. Therefore, in-depth study of the thermal conduction in DNA is important to clarify the denaturation mechanism via thermal fluctuations.

1.4. Scope of present work

Systematic work is conducted to investigate the thermal transport in DNA with comprehensive thermal characterization techniques. Chapter 2 reports on the synthesis of salmon testes DNA-composited microfiber and microfilm, and details the study of thermal transport in them at room temperature. In Chapter 3, an extensive thermal transport study along the DNA microfiber is carried out from room temperature to low temperature (10 K). Temperature variations of the thermo-physical properties for DNA microfiber shed more light on the thermal transport in DNA. Particularly, a new theory based on "thermal reffusivity", the inverse of thermal diffusivity, is established to quantitatively evaluate phonon scattering induced by structural defects. The structural size for defect-induced phonon scattering in DNA microfiber is determined for the first time. In Chapter 4, thermo-physical properties for a λ-DNA nanofiber with a diameter of 464 nm are reported at 27~301 K. Compared to microfiber, the λ-DNA nanofiber has the great potential to possess a higher

thermal conductivity since more oriented DNA and less structural defects are anticipated. The thermal reffusivity theory is also updated without using single relaxation time approximation. In Chapter 5, novel DNA nanofiber array fabrications are developed to enable the thermal transport study on DNA nanofiber with a diameter of around 100 nm or less. Thermal characterizations of a DNA nanofiber with a diameter of 150 nm are reported. Conclusion of this work is summarized in Chapter 6. Guidance for future work is provided afterwards.

CHAPTER 2. THERMAL TRANSPORT IN CRYSTALLINE DNA MICRO-COMPOSITES

This chapter reports on the synthesis of microscale DNA-composited fiber and film, and details the study of thermal transport in them at room temperature. Comprehensive thermal characterization techniques are introduced for understanding the thermal transport in the DNA micro-composites. The transient electro-thermal (TET) technique is applied to characterize the thermal transport in DNA-composited microfiber, and the photothermal technique is used to explore the thermal transport in the thickness direction of DNA-composited microfilm. Sample preparation is described in Section 2.1. In Section 2.2 and 2.3, the TET and photothermal technologies are introduced respectively. Results are reported in Section 2.4, followed by analysis of structure and physics.

2.1. Sample preparation

2.1.1. Preparation of DNA-TE buffer solution

DNA from salmon testes (~2 kbp, Sigma-Aldrich) and sodium chloride (NaCl) are dissolved in TE (10 mM Tris-HCl and 1.0 mM EDTA) buffer. Under natural conditions, the negative charges from phosphate groups (PO_4^{3-}) on DNA cause DNA molecules to repel each other. However, NaCl provides Na^+ ions that will "screen" some of the negative charges, allowing DNA molecules to get close enough to form DNA bundle. In fact, DNA fibers are unable to be fabricated without the use of NaCl in this Chapter. Because of the addition of NaCl, the prepared samples are not DNA but DNA-NaCl composite. Solutions with two concentrations are used: in Group 1 solution, 0.5 wt% DNA with 5 wt% NaCl is used,

followed by the instructions for generating DNA nanostrands.[21] Group 2 solution is 1 wt% DNA with 1 wt% NaCl to have a lower NaCl concentration but a higher DNA concentration. The Group 2 solution is more viscous due to the higher DNA concentration. Prepared DNA solutions are stored in a freezer at −20°C and will be thawed before use.

2.1.2. Synthesis of DNA-composited microfiber

The method for drawing suspended fiber from liquid polymer[22] is modified for fabricating suspended DNA-composited microfiber, as illustrated in Fig. 2.1. Two DNA droplets are first transferred onto two copper electrodes by using a Pasteur pipette [Fig. 2.1(a)]. When the DNA solution reaches consistency through evaporation, a tungsten tip (tip diameter: 25 μm) is dipped into one droplet by any available angle, and the DNA fiber can be most easily hand-drawn out at the edge of the droplet, as shown in Fig. 2.1(b). The drawn fiber will be attached to the second droplet and dissolve from the tip [Fig. 2.1(c)]. The entire fiber continues to dry to form a suspended fiber [Fig. 2.1(d)]. The length and diameter of the fiber are evaluated under a scanning electron microscope (SEM) [Fig. 2.1(e)]. The length is mainly determined by the preset gap distance and the direction of the drawing process with respect to the electrode edges. By contrast, the diameter of the fiber is not well-controlled. Although it is believed that the diameter will increase with the solution viscosity as the solution dries,[22] the hand drawing process is incapable of producing fibers out of the solution repeatedly at a similar solution viscosity, even with the same concentration of initial solution. As listed in Table 2.1, all fibers are microfibers with a diameter in a wide range of 1 to 15 μm. Nevertheless, all fibers are round and uniform over the whole fiber length, same as the one presented in Fig. 2.1(e).

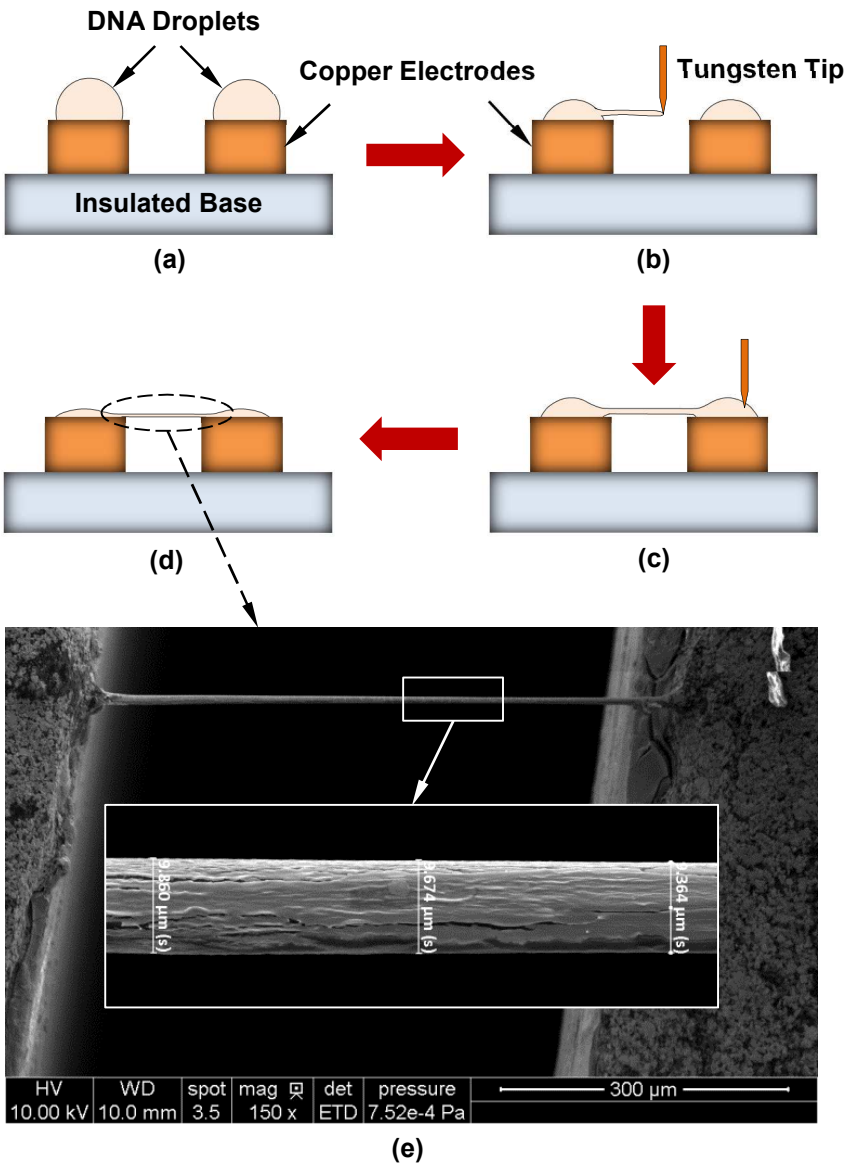

Figure 2.1. Fabrication of suspended DNA-composited microfiber: (a) DNA droplets are dropped onto the electrodes; (b) a tungsten tip is dipped into one droplet, and the fiber can be most easily hand-drawn out at the edge of the droplet; (c) the fiber will be attached to another droplet and dissolve from the tip; (d) the entire fiber continues to dry to form a suspended fiber. (e) SEM image of a well-formed DNA-composited microfiber from Group 1 solution.

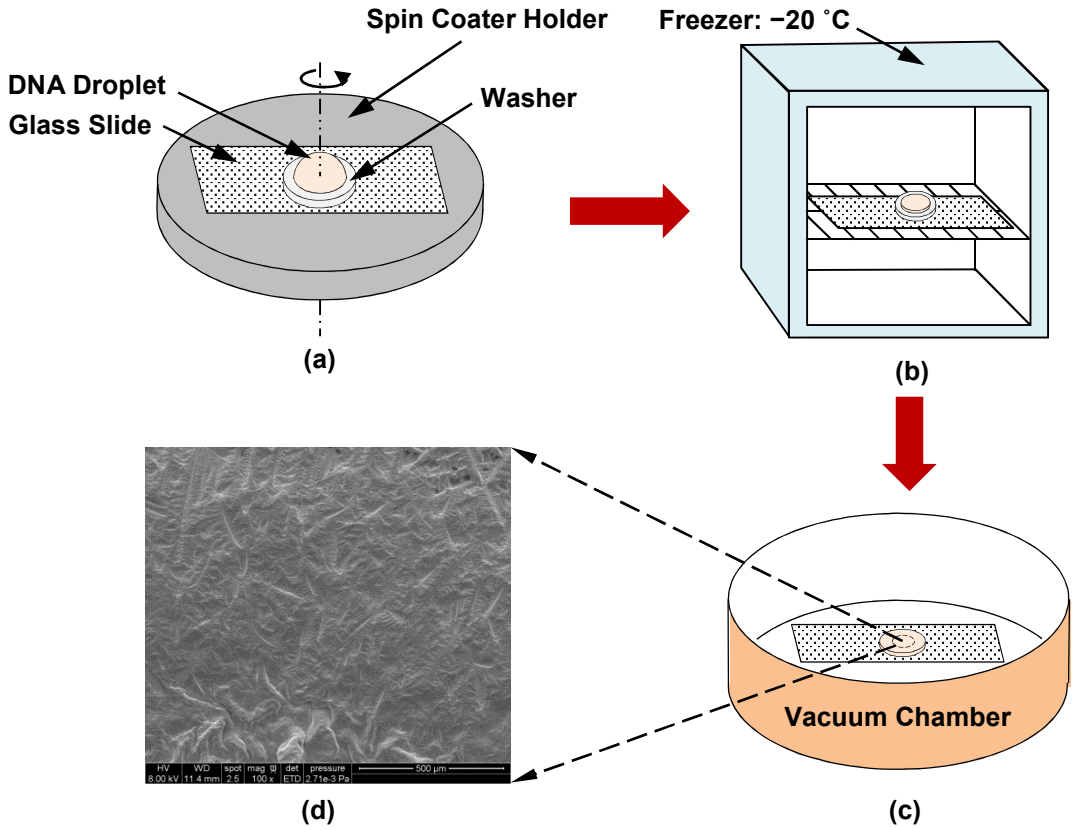

Figure 2.2. Fabrication of uniform DNA-composited microfilm: (a) DNA solution is dropped inside a washer taped to a glass slide, and then spins with the slide in a spin coater to make the droplet uniform in the lateral direction; (b) the droplet is frozen at −20°C for several minutes and then the washer is taken off, and the droplet continues to be frozen at the same temperature for 1 hour; (c) the moisture is removed through the process of sublimation by placing the frozen sample in a vacuum chamber down to 100 mTorr for another hour. (d) SEM image of uniform region of a DNA-composited microfilm.

2.1.3. Synthesis of DNA-composited microfilm

Figure 2.2 shows the fabrication of DNA-composited microfilm from DNA solution. The film thickness is an important parameter in the measurement. However, a major

challenge during the fabrication is that the film is not uniform in the thickness direction due to the formation of uneven dendritic film textures (Fig. 2.3). It is found that the dendritic textures are induced by Na^+ ions with the evaporation of solution.[23] Once the concentration of Na^+ ions reaches maximum as evaporation, subsequent evaporation of the solution will lead to the association of Na^+ and Cl^- ions. Since Na^+ ions are also tethered to the phosphate groups, the sedimentation will cause the crystallization of DNA-NaCl complexes. As shown in Fig. 2.3, the presence of dendritic textures makes the DNA film uneven in thickness. To improve the uniformity, the film is attempted to be fabricated through sublimation other than evaporation. Hence, following steps are developed accordingly. A DNA solution is first dropped inside a washer taped to a glass slide. The slide carried with the solution then spins in a spin coater to make the droplet uniform in the lateral direction [Fig. 2.2(a)]. Second, the droplet is frozen at −20°C for several minutes and then the washer is taken off, and continues to be frozen at the same temperature for 1 hour [Fig. 2.2(b)]. Then the moisture is removed through the process of sublimation by placing the frozen sample in a vacuum chamber down to 100 mTorr for another hour [Fig. 2.2(c)]. This is a common strategy to dehydrate frozen materials in freeze-drying.[24] Above approaches cannot completely exclude dendritic textures in DNA film. However, it is beyond the point whether or not the film contains dendritic textures since the goal is to make uniform film. In fact, the dendritic textures are appreciated with the crystalline DNA-NaCl complexes favorable for thermal transport. Most uniform and condensed region of the film is chosen for the measurement, as shown in Fig. 2.2(d). The average thickness of the measured film region is characterized by using a profilometer (Zygo NewView 7100). As listed in Table 2.2, all films are microfilms with a thickness in a range of 10~40 μm.

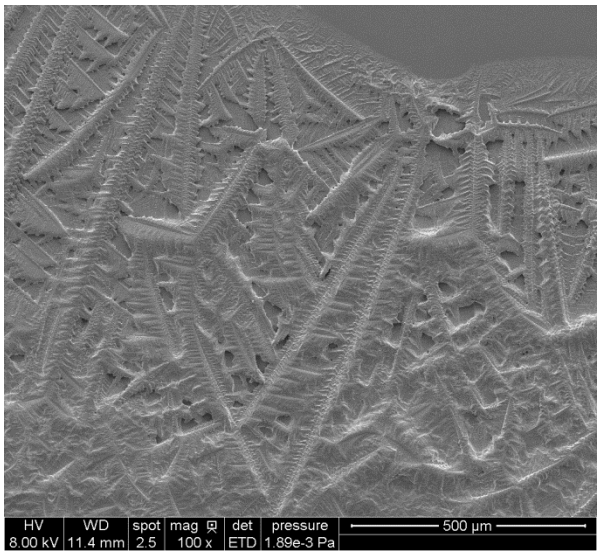

Figure 2.3. Dendritic DNA film textures.

2.2. Transient electro-thermal (TET) technique

2.2.1. Physical and experimental principles

Throughout this work, evaluations of thermo-physical properties of DNA are focused on: thermal conductivity k, volumetric heat capacity (product of density and specific heat, ρc_p), and thermal diffusivity $\alpha = k / \rho c_p$. Thermal conductivity, of course, is the most common property and thus receives most attention. However, thermal conductivity is not consistently measured in this work. Another common approach to obtain thermal conductivity is to measure thermal diffusivity and volumetric heat capacity separately, and the thermal conductivity can be calculated afterwards. Meanwhile, thermal diffusivity and volumetric heat capacity have their own importance. Thus, having their values is also vital to decode the thermal transport process in DNA.

In this work, the TET technique is applied to measure the thermal diffusivity of DNA-composited microfiber. This technique is capable of evaluating the thermal diffusivity of micro/nanoscale wires and fibers.[25-38] For example, Guo *et al.*[25] measured the thermal diffusivity of Pt wire as 2.53~2.78×10^{-5} m^2/s by using the TET technique, in agreement with the literature value 2.51×10^{-5} m^2/s. The experimental principle of the TET technique is shown in Fig. 2.4(a). In the TET technique, the sample suspended between two electrodes is fed a periodic step dc current with joule heating ($Q = I^2 R$). For electrical insulating materials such as DNA-composited microfiber, a thin (nano-meter thick) metal film needs to be coating with the materials to apply the TET technique. In this case, a thin gold film is sputtering coated (DESK V, Denton Vacuum) on the top side of the fiber. The temperature rise evolution due to the heating can be monitored through the voltage increase across the sample, given constant feeding current and temperature coefficient of resistance. A typical voltage increase profile recorded by a digital oscilloscope is presented in Fig. 2.4(b). When the current is "on", the voltage will jump to an initial value V_0 and subsequently increase from V_0 to the steady state V_1 via a transient phase, indicating the temperature of the sample has been elevated. The transient phase of the profile can be used to determine the thermal diffusivity of the sample.

The physical model of the TET technique is validated as 1-D heat transfer along the sample's axial direction. The governing equation is

$$(\rho c_p)_s \frac{\partial T}{\partial t} = k_s \frac{\partial^2 T}{\partial x^2} + q_0 - \frac{4\varepsilon_r \sigma (T^4 - T_0^4)}{D}, \qquad (2\text{-}1)$$

where $(\rho c_p)_s$ and k_s are the volumetric heat capacity and thermal conductivity of the gold-coated sample. q_0 is the electrical heating power per unit volume, written as I^2R_0 / A_s where A_s is the cross sectional area of the sample. In the last term, σ=5.67×10^{-8} W/m^{2}K^4 is the Stefan-Boltzmann constant, and ε_r is the surface emissivity of the gold-coated sample. The emissivity of the coated half is 0.02~0.03, and the uncoated half is ~0.9 for biomaterials.[39] So the overall ε_r is estimated as 0.46. D is the sample's average diameter. In the measurement, the sample can be considered uniform if there are no bottlenecks for the energy transport along the fiber's axial direction. Same as the fibers shown in Fig. 2.1(e), 2.6(b) and 2.6(c), all DNA-composited microfibers are uniform without bottlenecks. For a particular sample, the average diameter is obtained by measuring the diameter at 10~20 locations along the fiber.

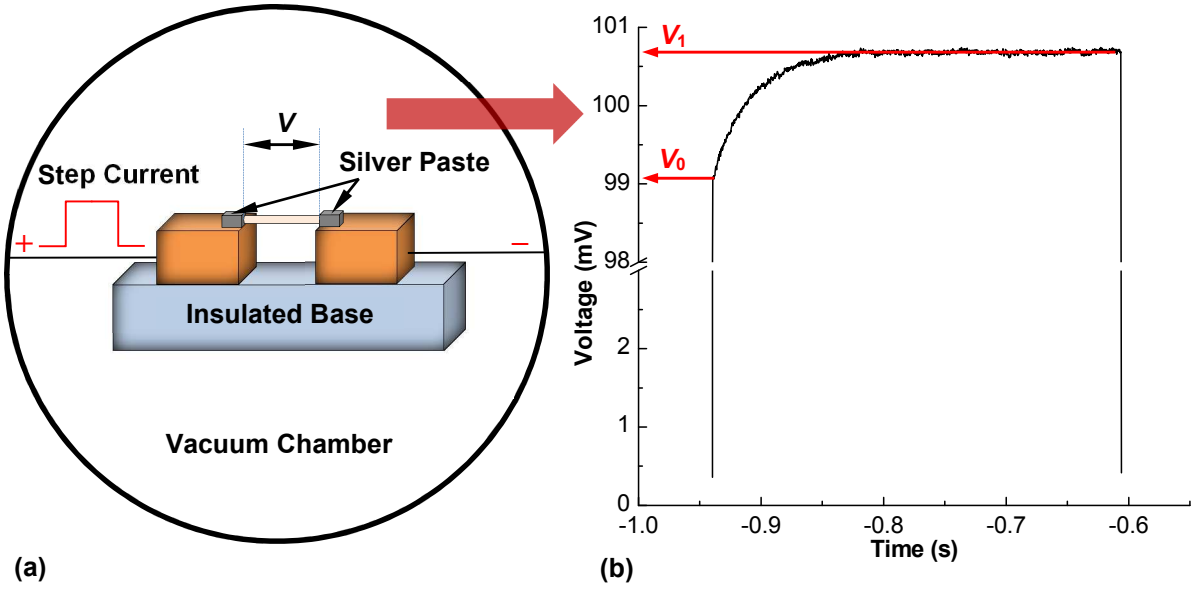

Figure 2.4. (a) Schematic of experimental principle of the TET technique. (b) A typical V-t profile in the TET technique.

The boundary conditions are described as $T(x=0,t)=T(x=l,t)=T_0$, where T_0 is the ambient temperature and l is the sample length. The initial condition is written as

$T(x,t=0)=T_0$. To validate the boundary conditions, the fiber ends are attached to large electrodes by using silver paste (PELCO colloidal silver, Ted Pella) to enhance the thermal conduction between them [Fig. 2.4(a)]. The thermal contact resistance is around 10^{-7}~10^{-8} m^2K/W for sound mechanical contact. For first order estimate, the thermal contact area can be assumed as the product of the contact length and the circumference of the sample's cross section embedded in the silver paste, which is around 10^{-9} m^2. So the absolute thermal resistance due to the contact is estimated to be around 100 K/W, negligible to the sample's thermal resistance (10^7~10^8 K/W). Therefore, the temperature at both sample ends can be considered to be equal to T_0 when heating is introduced. Meanwhile, the electrical contact resistance is reduced to only a few ohms with applying silver paste for the 2-probe method, negligible to the sample's electrical resistance (a few hundred ohms to a few thousand ohms).

Additional information regarding the experimental setup is as follows. The sample is tested in a vacuum chamber whose pressure is 1~3 mTorr (detected by a convection vacuum gauge, CVM 211 Stinger, InstruTech), since the heat convection and conduction by air are eliminated from the physical model. In addition, the heating power per unit volume q_0 is assumed constant in the model. However, q_0 will increase as the electrical resistance increases. If the resistance increase is significant, q_0 has to be written as $I^2R_0[1+\varepsilon(T-T_0)]/A_s$ instead of I^2R_0/A_s, where ε is the temperature coefficient of resistance (TCR). This will increase the complexity of solving the equation. As a consequence, q_0 is elaborately controlled in the experiment by selecting a good current value. Usually the loading current should make sure that the electrical resistance increase is 0.6~2%, large enough to have distinct voltage increase profile and small enough to maintain the

constant heating assumption. Controlling the heating is also aimed to have the experiment conducted with a small temperature rise. Thus the thermal diffusivity can be considered constant within the temperature range. In general, the temperature rise in the TET technique is found to be 8~15 K in this work.

2.2.2. Radiation effect

In the original physical model developed by Guo *et al.*,[25] there is no last term entitled "radiation effect" at the right hand side of Eq. (2-1). The solution to the original version of governing equation is expressed in normalized temperature $T^*(t)$, defined as $T^*(t)=[T(t)-T_0]/[T(t\to\infty)-T_0]$,

$$T^*(t)=\frac{96}{\pi^4}\sum_{i=1}^{\infty}\frac{1-\exp[-(2i-1)^2\pi^2\alpha_s t/l^2]}{(2i-1)^4}, \tag{2-2}$$

where α_s is the thermal diffusivity of the gold-coated sample. The experimental normalized voltage increase V^*, defined as $[V(t)-V_0]/[V_1-V_0]$, can be fitted to T^* with α_s by the least square method. However, it turns out that the radiation effect cannot be ignored in this work. With the addition of radiation effect term, it requires more derivations to obtain the analytical solution similar to Eq. (2-2), where α_s is replaced by effective thermal diffusivity α_{eff} in which the radiation effect is included as additional equivalent thermal diffusivity.

First, the radiation effect term in Eq. (2-1) is simplified as $a\theta$ by introducing $\theta=T-T_0$ for $\theta<<T_0$ and $a=16\varepsilon_r\sigma T_0^3/D$. Then by defining a new parameter $f=al^2/\pi^2k_s$ and substituting $\theta=\varphi\exp(-f\pi^2\alpha_s t/l^2)$, the governing equation can be rewritten as

$$(\rho c_p)_s \frac{\partial \varphi}{\partial t} = k_s \frac{\partial^2 \varphi}{\partial x^2} + q_0 \exp(\frac{f \pi^2 \alpha_s t}{l^2}). \quad (2\text{-}3)$$

Now the equation takes the same form as the original version without radiation effect term so that it can be solved by integral of the same Green's function described in Guo *et al.*'s work [25]. Then the average temperature across the sample can be integrated as

$$T(t) = \frac{1}{l}\int_{x=0}^{l} T(x,t)dx = T_0 + \frac{8q_0 l^2}{k_s \pi^4} \sum_{i=1}^{\infty} \frac{1 - \exp\left\{-\left[f + (2i-1)^2\right]\pi^2 \alpha_s t / l^2\right\}}{[f + (2i-1)^2](2i-1)^2}. \quad (2\text{-}4)$$

For the steady state ($\partial T / \partial t = 0$), let $m = \sqrt{a / k_s}$ and $\psi = \theta - q_0 / a$, and the steady state governing equation becomes

$$\frac{\partial^2 \psi}{\partial x^2} - m^2 \psi = 0. \quad (2\text{-}5)$$

This is identical to the equation for heat transfer problem with a fin of uniform cross-sectional area. The boundary condition at the fin tip (the center of the sample) is adiabatic, i.e. $\frac{\partial \psi}{\partial x}|_{x=2/l} = 0$. So the average steady state temperature is obtained as

$$T(t \to \infty) = T_0 + \frac{q_0}{a}[1 - \frac{\tanh(ml/2)}{ml/2}], \quad (2\text{-}6)$$

and can be simplified as

$$T(t \to \infty) \cong T_0 + \frac{q_0}{a}[\frac{1}{3}(\frac{ml}{2})^2 - \frac{2}{15}(\frac{ml}{2})^4] = T_0 + \frac{q_0 l^2}{12 k_{eff}} \quad (2\text{-}7)$$

when $\left|\frac{ml}{2}\right| < \frac{\pi}{2}$, which is valid for DNA samples in this work. In Eq. (2-7), the effective thermal conductivity is introduced as $k_{eff} = k_s + 8\varepsilon_r \sigma T_0^3 l^2 / 5D$. Combining Eqs. (2-4) and (2-7), the normalized temperature can be written as

$$T^* = \frac{96}{\pi^4}\sum_{i=1}^{\infty}(1+\pi^2 f/10)\frac{1-\exp\left\{-(2i-1)^2\left[f/(2i-1)^2+1\right]\pi^2\alpha_s t/l^2\right\}}{[f/(2i-1)^2+1](2i-1)^4}. \quad (2\text{-}8)$$

For $\frac{f}{(2i-1)^2} \approx 0$, T^* can be simplified as

$$\begin{aligned} T^* &= \frac{96}{\pi^4}\sum_{i=1}^{\infty}(1+\pi^2 f/10)\frac{1-\exp\left\{-(2i-1)^2\pi^2\alpha_s t/l^2\right\}}{(2i-1)^4} \\ &= \frac{96}{\pi^4}\sum_{i=1}^{\infty}\frac{1-\exp\left\{-(2i-1)^2\pi^2\alpha_{eff} t/l^2\right\}}{(2i-1)^4}. \end{aligned} \quad (2\text{-}9)$$

where $\alpha_{eff} = \alpha_s(1+\pi^2 f/10) = \alpha_s + 8\varepsilon_r\sigma T_0^3 l^2/5D(\rho c_p)_s$. Now T^* takes the same form as Eq. (2-2). The new fitting parameter, α_{eff}, is the sum of the thermal diffusivity of sample and additional equivalent thermal diffusivity induced by radiation.

2.2.3. Lorenz number

The thermal diffusivity of the sample α_s can be further decomposed as

$$\alpha_s = \frac{k(1-\chi)+k_f\chi}{\rho c_p(1-\chi)+(\rho c_p)_f\chi}, \quad (2\text{-}10)$$

where k and ρc_p are the thermal conductivity and volumetric heat capacity of DNA-composited fiber, k_f and $(\rho c_p)_f$ are the thermal conductivity and volumetric heat capacity of thin gold film. $\chi = A_f/A_e$ is the cross-sectional ratio of gold film, where A_f is the cross-sectional area of thin gold film. Using the Wiedemann-Franz law, k_f can be evaluated based on electrical resistance R_0, and for $\chi \approx 0$,

$$\alpha_s = \alpha + \frac{L_{Au}T_0 l}{R_0 A_e \rho c_p}, \quad (2\text{-}11)$$

where L_{Au} is the Lorenz number for gold film. As a result, the thermal diffusivity of DNA fiber can be expressed as

$$\alpha = \alpha_{eff} - \frac{L_{Au} T_0 l}{R_0 A_e \rho c_p} - \frac{8\varepsilon_r \sigma T_0^3 l^2}{5\rho c_p D}. \quad (2\text{-}12)$$

The Lorenz number for bulk gold is 2.35×10^{-8} WΩ/K^2 at 273 K and 2.40×10^{-8} WΩ/K^2 at 373 K.[40] However, the values for bulk gold are not taken for granted in this work, since evidence has shown that the Lorenz number for nanoscale gold film may be much higher than the bulk's value.[41-43] In fact, the Lorenz number for thin gold film at room temperature can be evaluated by using the TET technique. In this work, the Lorenz number of 20~60 nm thick gold film is measured by using spider silk fiber samples as substrates (*Nephila clavipes* and *Latrodectus hesperus*). The procedure is to measure α_{eff} with accumulated gold coatings. First, the fiber sample is coated with a thin gold film, and the TET measurement is conducted to measure α_{eff}. Then the sample is coated with another gold film on the top of the previous gold film, and the TET experiment is conducted again under the same experimental conditions. The same process is repeated until sufficient data have been collected to do the fitting. The α_{eff}~$1/R_0$ plot can be fitted with Eq. (2-12). With other known parameters, the Lorenz number for thin gold film is determined as 2.27×10^{-8} WΩ/K^2 at room temperature, close to the bulk's value.

The volumetric heat capacity ρc_p of DNA-composited microfiber is needed in Eq. (2-12) to subtract radiation and gold effects as well as to extract Lorenz number of gold film for the Lorenz number determination. However, ρc_p cannot be obtained in the TET technique. Meanwhile, the thermal conductivity of DNA-composited microfiber is unable to be

extracted. By contrast, ρc_p of DNA-composited microfilm is measured by the photothermal technique introduced in the next section. For each group the fiber and film are from the same solution, so they can be reasonably considered to share the same value of ρc_p. Therefore, the value of ρc_p obtained from the photothermal technique for DNA-composited microfilm is used as that for DNA-composited microfiber. The thermal conductivity of the fiber is calculated afterwards.

2.3. Photothermal technique

Thermo-physical properties of DNA-composited microfilm are evaluated by using the noncontact photothermal technique.[44-48] This measurement is also intended to provide the data of ρc_p that can be used to process the DNA-composited microfiber results to obtain its thermal diffusivity and thermal conductivity, as described in the previous section. A schematic of the photothermal technique is shown in Fig. 2.5. In the experiment, a continuous infrared diode laser (BWTEK BWF-2, 809 nm wavelength) modulated by a function generator is directed and focused on the film to induce periodic heating and temperature variation at the film surface. To have the laser beam absorbed on the surface in a controlled way, a 50 nm-thick gold film is sputtering coated on top of the film. The temperature variation due to the laser heating is strongly dependent on the thermo-physical properties of the film. When the temperature variation is not very large, it has a linear relationship with the change of the thermal radiation as $\Delta Q \propto 4\varepsilon_r \sigma T_0^3 \Delta T$. Therefore, the temperature variation can be sensed by measuring the thermal radiation from the film surface, which is directed to an infrared detector. In order to filter out the reflected laser beam, a Ge window is placed in front of the detector to allow thermal radiation to pass only. The signal

from the infrared detector is pre-amplified and then measured by a lock-in amplifier. The experiment is controlled by a computer for automatic data acquisition.

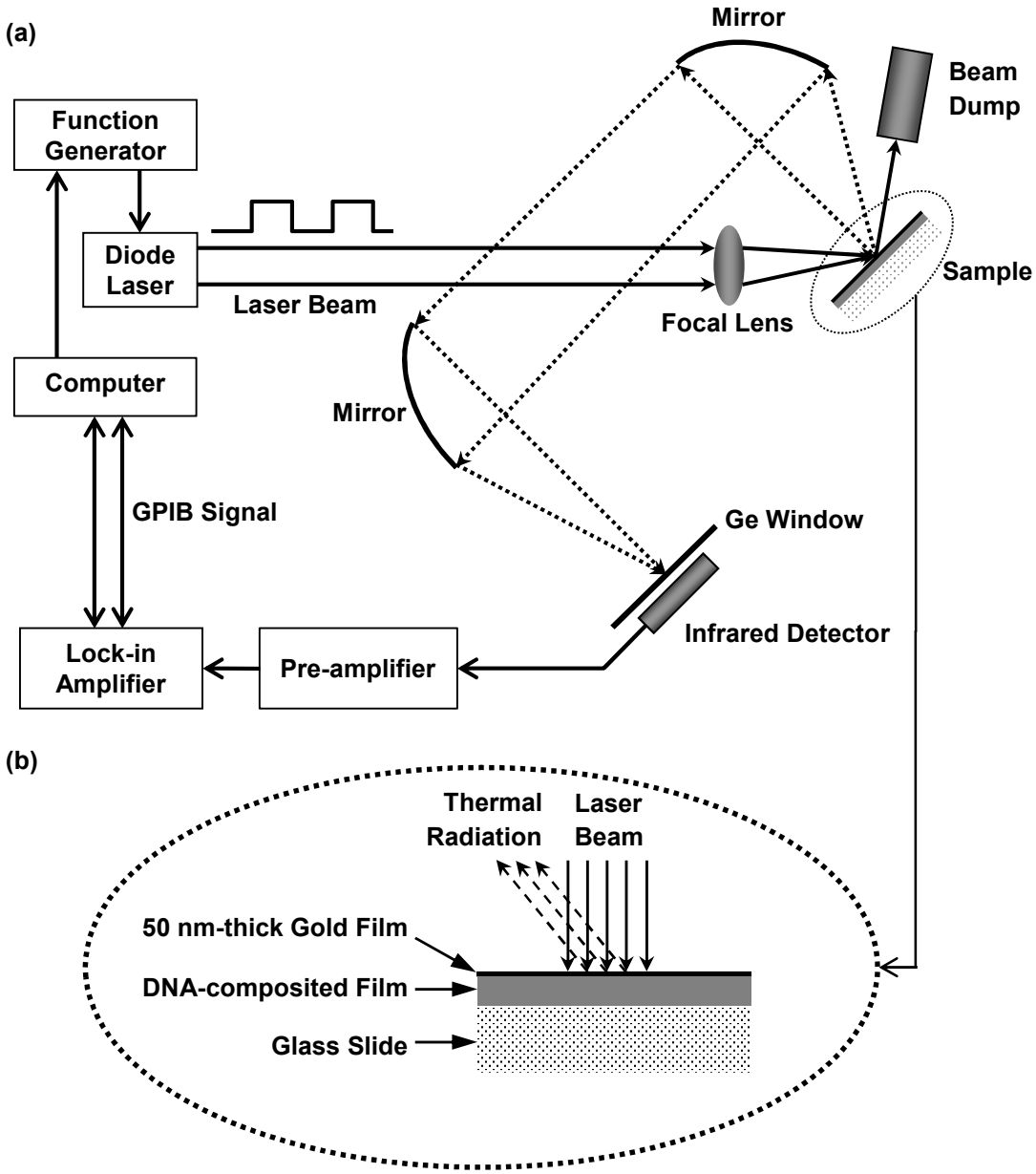

Figure 2.5. (a) Schematic of the experimental setup for the photothermal technique and (b) the structure of DNA-composited microfilm sample.

The heating source in the photothermal technique is assumed to be a sinusoidally modulated monochromatic laser beam of wavelength λ with a flux of $J = J_0(1+\cos\omega t)/2$, where ω is the modulation frequency of the incident laser beam. The one-dimensional thermal diffusion equation in layer i for an N-layer sample is given by

$$\frac{\partial^2\theta_i}{\partial x^2} = \frac{1}{\alpha_i}\frac{\partial\theta_i}{\partial t} - \frac{\beta_i J_0}{2k_i}\exp\Big(\sum_{m=i+1}^{N} -\beta_m L_m\Big)\,e^{\beta_i(x-l_i)}(1+e^{j\omega t}), \tag{2-13}$$

where α_i, β_i and k_i are the thermal diffusivity, optical absorption coefficient and thermal conductivity of layer i, respectively. $L_i = l_i - l_{i-1}$ and $\theta_i = T_i - T_0$ are the thickness and modified temperature in layer i. The solution to the equation has three parts: an initial transient component $\theta_{i,t}$, a steady dc component $\overline{\theta}_{i,s}$, and a steady ac component $\tilde{\theta}_{i,s}$. The ac component of temperature distribution at the film surface, picked up by the lock-in amplifier, is expressed as

$$\tilde{\theta}_{N+1,s} = B_{N+1}e^{j\omega t}, \tag{2-14}$$

where B_{N+1} is the coefficient described in Ref.[44] In particular, the phase shift (ϕ) between the temperature at the film surface and the modulated laser beam contains the information of the thermo-physical properties for the film. Therefore, the phase shift between the thermal radiation and the modulated laser beam can be used to determine the thermo-physical properties of the DNA-composited microfilm. After the experiment, trial values of unknown properties such as thermal conductivity and interface resistance will be used to calculate the theoretical phase shift and compare it with the measured phase shift at each modulation frequency. The trial values giving the best fit of the experimental results (the least square method) will be taken as the properties of the sample.

Additional information regarding the photothermal technique is as follows. First, the system will inevitably introduce a phase shift (ϕ_{cal}) by itself, which needs to be calibrated by measuring the reflected laser beam from the sample. Second, the modulation frequency is set between 17 Hz and 20 kHz in the experiment. The spot of the laser beam is about 0.7 mm×1.4 mm (the beam is not perpendicular to the sample surface), which is larger than the thermal diffusion depth in the lateral direction of the sample within the frequency range. As a result, the thermal transport induced by laser heating can be treated as one-dimensional along the thickness direction of the film.

2.4. Results and discussion

2.4.1. Thermal transport in DNA-composited microfiber

For DNA-composited microfiber with roughly 40 nm-thick gold coating, the *I-V* curve is checked to be linear. Coherent quantum tunneling and diffusive thermal hopping effects for electron transport in DNA are not observed. Hence, TET technique can be properly applied for the thermal characterization in DNA-composited microfiber.

The samples are divided into two groups in terms of initial DNA solution: Group 1 contains fibers and films from the solution with 0.5 wt% and 5 wt% NaCl, and the composites in Group 2 are from the solution with 1 wt% DNA and 1 wt% NaCl. There are 8 and 5 DNA-composited microfibers in Group 1 and Group 2 respectively. Though the length and diameter of a particular fiber cannot be fully controlled, the size effects on thermal transport are addressed in the radiation and gold coating effects that are subtracted in the data processing. As a consequence, the thermal conductivity and diffusivity are independent of the

fiber size from the measurement aspect. Figure 2.6(a) shows the comparison between the best fitting curve with α_{eff} and experimental normalized temperature rise for two fibers in both groups (presented in log axis). The uncertainty of the fitting process is also illustrated by plotting another two fitting curves with ±10% variation of α_{eff}. It is conclusive that the percentage uncertainty of the fitting process is below 10%. For multiple measurements, the average result of α_{eff} has an uncertainty even smaller (~2%). The average value of α_{eff} for each fiber is taken as the experimental result shown in Table 2.1. Then the radiation and gold coating effects are subtracted to obtain the thermal diffusivity of DNA-composited microfiber. To do this, the volumetric heat capacity of the fiber is required. From the photothermal characterization on DNA-composited microfilm (Table 2.2), the average values of the volumetric heat capacity are determined as 1.25×10^6 J/m^{3}K for Group 1 samples and 1.21×10^6 J/m^{3}K for Group 2 samples. To the end, the thermal conductivity of DNA-composited microfiber is calculated through the definition $k = \alpha\rho c_p$.

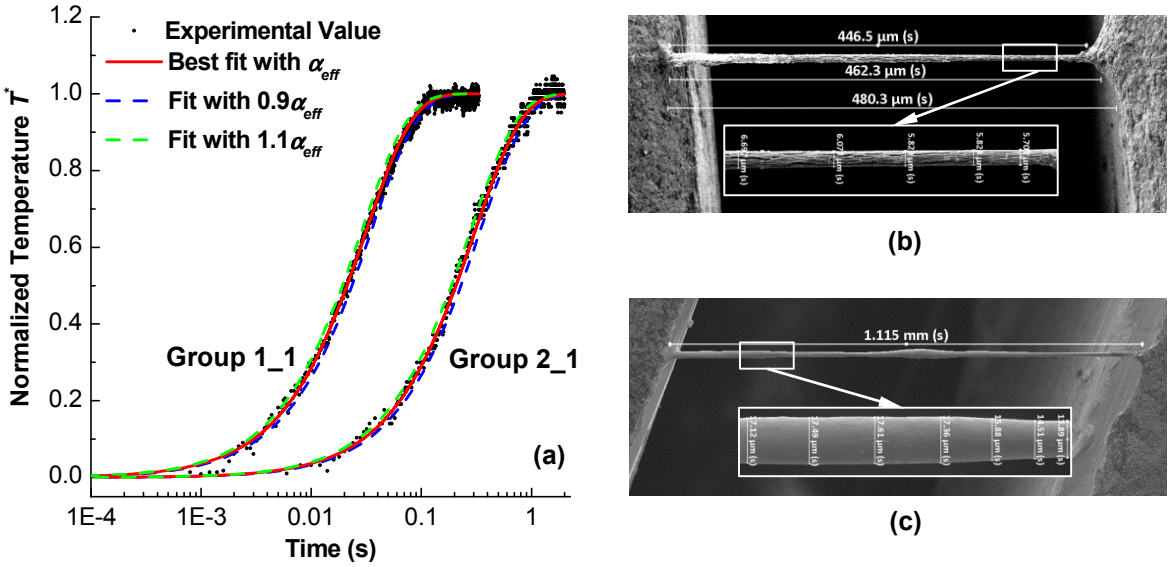

Figure 2.6. (a) TET fittings for DNA-composited microfibers. (b) SEM image of the fiber entitled “Group 1_1”. (c) SEM image of the fiber entitled “Group 2_1”.

Table 2.1. Experimental results for DNA-composited microfibers

Fiber	l (mm)	D (μm)	α_{eff} (10^{-7} m^2/s)	α (10^{-7} m^2/s)	k (W/m·K)
Group 1_1	0.447	8.32	6.33±0.63	4.67±0.63	0.76±0.10
Group 1_2	0.613	6.42	7.17±0.06	5.15±0.06	0.84±0.01
Group 1_3	0.778	3.84	6.11±0.12	2.97±0.12	0.48±0.02
Group 1_4	0.56	3.19	10.13±0.11	5.48±0.11	0.89±0.02
Group 1_5	0.448	5.50	3.97±0.01	2.26±0.01	0.37±0.00
Group 1_6	0.621	3.90	8.39±0.14	5.19±0.14	0.85±0.02
Group 1_7	0.536	5.58	6.17±0.17	2.94±0.17	0.48±0.03
Group 1_8	0.648	7.34	4.14±0.09	2.19±0.09	0.36±0.01
Group 2_1	1.115	15.16	4.17±0.08	1.92±0.08	0.33±0.01
Group 2_2	0.397	1.31	10.31±0.19	1.94±0.19	0.33±0.03
Group 2_3	0.515	8.39	2.76±0.03	1.42±0.03	0.24±0.01
Group 2_4	0.435	5.27	4.82±0.07	2.69±0.07	0.46±0.01
Group 2_5	0.534	8.24	3.13±0.04	1.62±0.04	0.28±0.01

2.4.2. Thermal transport in DNA-composited microfilm

4 and 3 DNA-composited microfilms in each group are measured by using the photothermal technique. The importance of film thickness has two aspects. First, two main parameters are determined directly in the photothermal technique: L/k, and $L\rho c_p$. Thus, the thermal conductivity and volumetric heat capacity are directly dependent on the thickness measurement accuracy. The uncertainty of the film thickness is shown in Table 2.2. By contrast, thermal effusivity defined as $\sqrt{k\rho c_p}$ is a parameter independent of the film thickness in the photothermal technique, which can also be compared between two group

films. Second, film structure can vary with film thickness. It is expected that a thicker film is easier to contain more pore structures. This structural effect can be evaluated by the thermal contact resistance between the film and glass substrate.

Table 2.2. Experimental results for DNA-composited microfilms

Film	L (μm)	ρc_p ($\times 10^6$ J/m^{3}K)	k (W/m·K)	$\sqrt{k\rho c_p}$ ($\times 10^3$ J/m^{2}Ks$^{0.5}$)	α (10^{-6} m^2/s)	R_{tc} (m^{2}K/W)
Group 1_1	36.21±0.17	1.244±0.126	7.40±0.75	3.072	6.00±0.85	1.0×10^{-9}
Group 1_2	38.13±0.17	1.631±0.163	15.53±1.56	5.033	9.52±1.35	1.0×10^{-9}
Group 1_3	13.37±0.20	1.011±0.102	20.69±2.09	4.574	20.46±2.93	1.3×10^{-7}
Group 1_4	26.85±0.41	1.108±0.112	12.40±1.25	3.707	11.19±1.60	1.0×10^{-9}
Group 2_1	23.65±0.30	0.993±0.100	3.65±0.37	1.904	3.67±0.52	8.9×10^{-6}
Group 2_2	36.03±0.54	1.094±0.111	3.29±0.33	1.896	3.00±0.43	4.4×10^{-5}
Group 2_3	22.62±0.31	1.556±0.157	2.05±0.21	1.786	1.32±0.19	5.4×10^{-5}

Figure 2.7(a) shows the phase shift fitting results against the experimental data for the film entitled “Group 1_1”. The fitting simultaneously determines the thermal conductivity and volumetric heat capacity. To evaluate the uncertainty of the fitting, two fitting curves with ±10% variation of the thermal conductivity with other fixed parameters are plotted. This shows that the percentage uncertainty of the fitting is less than 10%. Then 10% is used as the uncertainty for the fitting to estimate the uncertainty of thermal conductivity and volumetric heat capacity. The thermal contact resistance (R_{tc}) at the interface of film/glass substrate is

also given. All results for the DNA-composited microfilms are listed in Table 2.2.

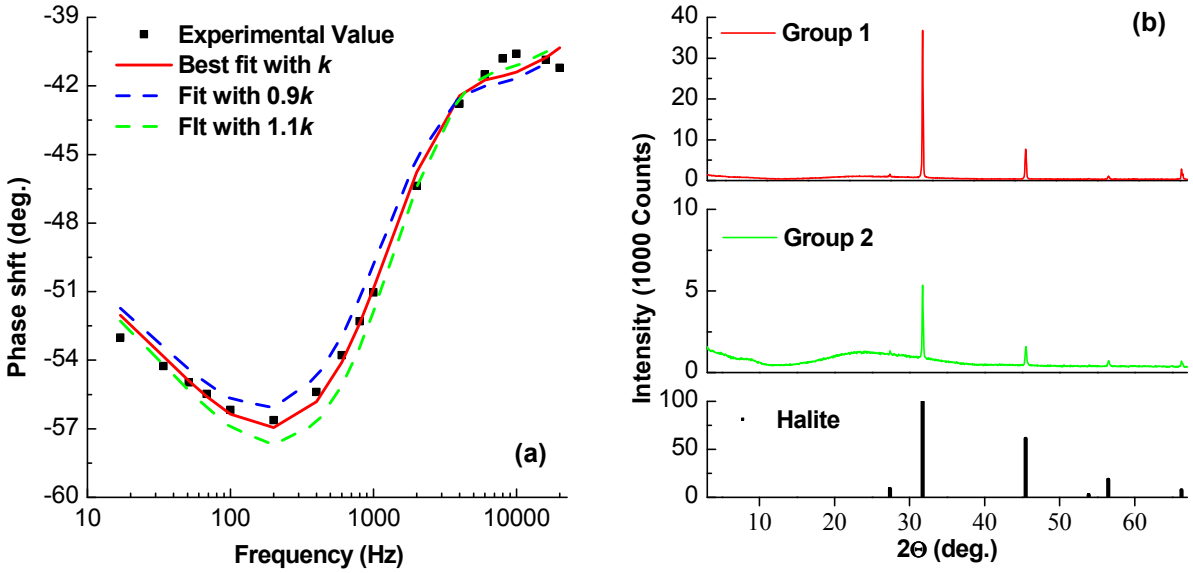

Figure 2.7. (a) Fitting of the phase shift for the film entitled "Group 1_1". Two fitting curves with ±10% variation of the thermal conductivity are plotted to show the uncertainty of the fitting. (b) XRD patterns of the DNA-composited microfilms in two groups. The bottom is the XRD pattern of Halite-NaCl for comparison.

2.4.3. Structure and physics behind the measurement results

The top and middle of Fig. 2.7(b) show the X-ray Diffraction (XRD) patterns of the DNA-composited microfilms in two groups. The scans are collected using the same parameters (a step size of 0.05 degrees and a dwell time of 3 seconds). The bottom of Fig. 2.7(b) is the reference XRD pattern of Halite-NaCl for comparison.[49] A profile fitting is used to determine precise peak positions and to estimate the crystallite size. The fitting results show that all peaks in both measured diffractograms match the reference Halite-NaCl pattern. In the meantime, the peaks in both diffractograms are too narrow to give reliable crystallite size estimates (larger than 100 nm), which indicates both films contain NaCl crystals with a

large crystallite size. The Group 2 film for XRD study is about 20 μm thick while the Group 1 film is about 10 μm thick. The NaCl concentration of the Group 1 solution is about twice of that for the Group 2 solution. Thus both films are expected to give similar peak height in XRD study if the fraction of NaCl in the film is the same as that in the solution. However, Fig. 2.7(b) shows that the Group 2 film has much lower peak intensity than the Group 1 film, indicating this film contains much less NaCl crystals. So the thermal transport in Group 2 film is expected to have less influence from NaCl. To check the thermal effect of NaCl, its thermal properties are summarized here. The density of NaCl is 2.17×10^3 kg/m^3, and its specific heat at 300 K is 859.2 J/kgK.[50] So the volumetric heat capacity of NaCl is 1.86×10^6 J/m^{3}K. The thermal conductivity of NaCl at 323 K is 5.6 W/m·K,[50] so the thermal diffusivity of NaCl is 3.0×10^{-6} m^2/s.

The films in two groups are compared in the first place. Group 1 film has higher thermal diffusivity and conductivity on average. Without considering the thickness measurement uncertainty, the thermal effusivity of Group 1 film is also higher. The thermal conductivity of Group 1 and Group 2 films are 14 W/ m·K and 3 W/ m·K respectively, and the thermal conductivity of NaCl is in between. As illustrated in XRD study, Group 1 film contains more NaCl crystals. Clearly having more NaCl crystals will increase the thermal conductivity of the film composite. However, it cannot explain why the thermal conductivity of Group 1 film is even higher than that of NaCl. It is proposed that the enhancement of thermal conductivity is due to the formation of crystalline DNA-NaCl complexes. Though great efforts have been put to generate uniform film structure by minimizing uneven dendritic textures, crystalline DNA-NaCl complexes are still formed in the most uniform area

of the film chosen for the measurement. The higher the concentration of Na^+ ions, the more crystalline DNA-NaCl complexes will be formed. As a consequence, the Group 1 films have a higher degree of crystallization, leading to higher thermal conductivity, diffusivity and effusivity.

Similarly, DNA-composited microfiber in Group 1 also has a higher thermal diffusivity and conductivity. The average thermal diffusivity and conductivity of fibers in Group 1 is 3.86×10^{-7} m^2/s and 0.63 W/m·K, higher than those of the fibers in Group 2 (1.92×10^{-7} m^2/s and 0.33 W/m·K). F-test shows that the difference between these two groups is statistically significant. The enhancement of the thermal conduction is also proposed by the formation of crystalline DNA-NaCl complexes as the films. With relatively higher NaCl concentration, the DNA solution of Group 1 could have a better chance to form fibers with a higher degree of crystallization, leading to higher thermal conductivity and diffusivity. The evidence for more crystallized DNA structures in the Group 1 fibers can be seen from the SEM images. It is observed that the fiber in Group 1 has evident and visible aligned fiber structure, while the fiber in Group 2 does not [Fig. 2.6(b) and (c)].

In the last, the thermal conductivity and diffusivity of the fiber are much lower than those of the film in each group. First, the crystallization occurred in the DNA fiber is speculated to be at a lower degree than that in the film. The fiber is drawn out of the solution when the solution has not dried out. So the concentration of Na^+ ions has not reached the maximum at the moment of drawing. This will lead to less crystalline DNA-NaCl complexes and reduce the thermal conduction in DNA fiber. In addition, the fiber could contain less

NaCl crystals while the film will have more. When the fiber is drawn, it is unlikely to have a lot of NaCl crystals been drawn simultaneously. By contrast, the film is formed with a lot of NaCl precipitating on the film. As a consequence, heat is mainly conducted through DNA fiber without NaCl since NaCl crystals are only discretely distributed on the fiber surface, as shown in Fig. 2.6(b) and (c). By contrast, heat is conducted through the film structure with NaCl in the thickness direction. Hence, NaCl will have more thermal effects in the DNA-composited microfilm than in the microfiber.

CHAPTER 3. ENERGY TRANSPORT IN DNA MICROFIBER DOWN TO 10 K

In this Chapter, an extensive study of thermal transport in DNA microfiber is reported from room temperature to low temperature (10 K). Temperature variation of thermo-physical properties for DNA microfiber will shed more light on the thermal transport in DNA. The DNA microfibers studied in this work are synthesized from Group 2 solution described in Section 2.1. The DNA fiber from this group is expected to have least thermal effect from NaCl among all four kinds of DNA samples discussed in Chapter 2. Section 3.1 begins with the descriptions of the cryogenic system for the measurement, and details how to simultaneously evaluate thermal conductivity, thermal diffusivity and volumetric heat capacity by applying the TET technique in the cryogenic system. Temperature variations of the thermo-physical properties for two DNA microfibers are reported in Section 3.2.3. In Section 3.2.4, the inverse of thermal diffusivity is introduced as "thermal reffusivity" to quantitatively determine the impact of structural defects on phonon scattering. In the meantime, the electrical conduction of iridium (Ir) nanoscale film coated on DNA microfiber are also studied in detail, and DNA-promoted electron transport is proposed in Section 3.2.1. The Lorenz number of Ir film over a wide temperature range is evaluated and discussed in Section 3.2.2.

3.1. Experimental details

3.1.1. Cryogenic system

An electrode base carried with DNA microfiber [Fig. 3.1(a)] is installed onto the sample mount of a cryogenic system [CCS-450, JANIS, Fig. 3.1(b)] for the thermal characterization. The system can be used to perform experiments under temperatures as low as 10 K. A closed loop of helium gas is compressed and expanded between the compressor and the cold head. During the expansion phase of each cycle, heat is removed from the cold finger, on which the electrode base carried with DNA microfiber is installed. The cold finger is covered by a radiation shield to block room temperature radiation before it reaches the sample, allowing the lowest possible sample temperature to be achieved. A heater and a thermometer are installed on the cold finger and are used to precisely control the sample temperature by a temperature controller. The system is connected to a cold-trapped mechanical vacuum pump to reach a vacuum level as low as 0.3 mTorr, which is needed to eliminate the heat convection and conduction by air in the measurement. For the sake of measurement, the electrode base is electrically insulated from the sample mount by applying a thin cryogenic vacuum grease (Apiezon N Grease) film between them. The grease film also provides a good thermal contact, making the sample temperature very close to that of the cold finger. The electrodes are connected to the electrical feedthroughs by using small gauge wires (32 AWG) for applying current to the sample and for voltage measurement across the sample.

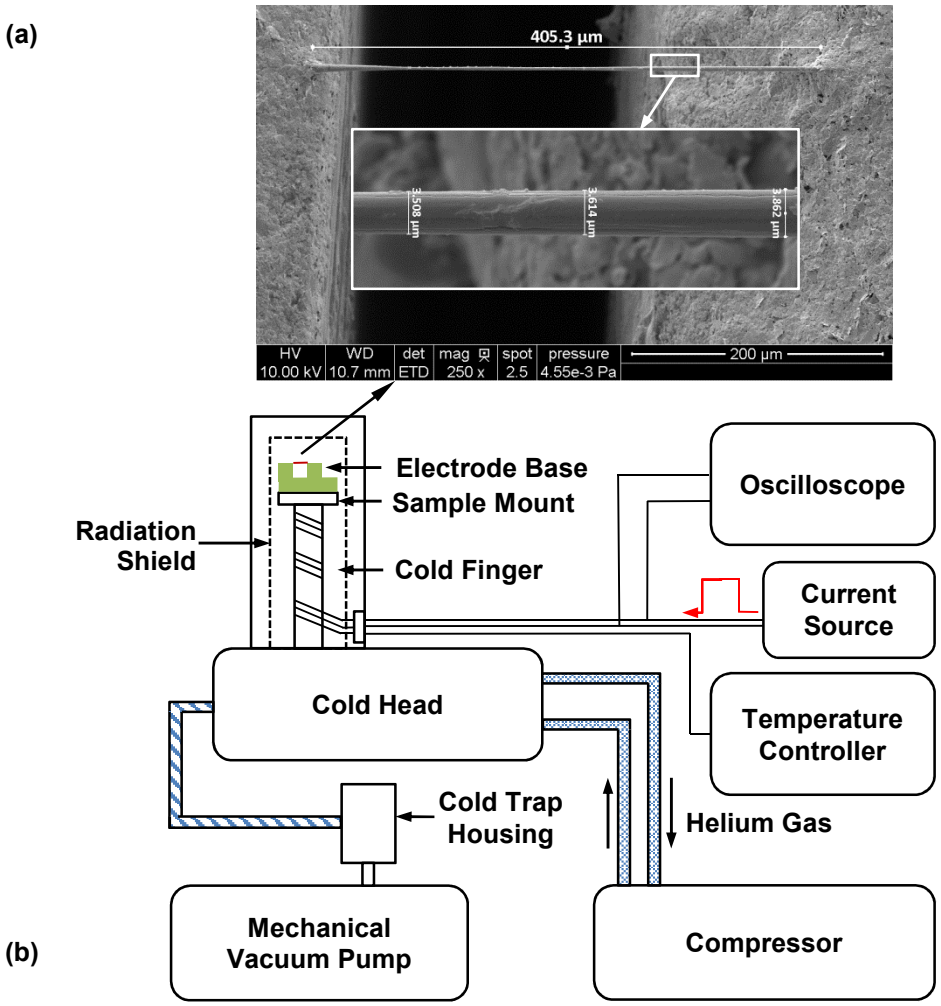

Figure 3.1. (a) SEM image of DNA fiber 1. (b) Schematic of the experimental setup in the cryogenic system. An electrode base is installed onto the sample mount in the cold finger. The temperature is precisely maintained by a temperature controller. The electrodes are connected to the electrical feedthroughs for applying current to the sample and for voltage measurement across the sample.

3.1.2. TET characterization in cryogenic system

Thermal conductivity, volumetric heat capacity and thermal diffusivity can be simultaneously determined by using the TET technique with a measurement of the

temperature coefficient of resistance (TCR) in the cryogenic system. Before the experiment, the DNA microfiber is coated with a 15 nm Ir film (Q150T, Quorum Technologies) to apply the TET technique. More details of the TET technique have been provided in Section 2.2. With TCR, the actual temperature rise due to the heating can be found. This is very different from applying the TET technique at room temperature. According to Eq. (2-7), the effective thermal conductivity k_{eff} can be obtained with the steady state temperature rise. Then the thermal conductivity of DNA microfiber k is obtained by subtracting the Ir and radiation effects from k_{eff},

$$k = k_{eff} - \frac{L_{Ir} T_0 I}{R_0 A_e} - \frac{8\varepsilon_r \sigma T_0^3 l^2}{5D}. \tag{3-1}$$

Note that the radiation effect is ignored at low temperatures (<150 K), since the radiation power is depressed to only a percentage of the electrical heating power. So the last term in Eq. (3-1) is set to zero when temperature is below 150 K. The effective thermal diffusivity α_{eff} is solved by fitting the experimental normalized voltage evolution to the theoretical solution $T^*(t)$, as shown in Eq. (2-9). The volumetric heat capacity (ρc_p) of DNA microfiber is given by $\rho c_p = k_{eff} / \alpha_{eff}$. To the end, the thermal diffusivity of DNA microfiber is solved by $\alpha = k / \rho c_p$.

3.2. Results and discussion

Two DNA microfibers are measured down to 10 K. The length and average diameter of DNA fiber 1 are 0.405 mm and 3.47 μm, as shown in Fig. 3.1(a). The length and average diameter of DNA fiber 2 are 0.703 mm and 13.9 μm, respectively. Both fibers are coated with a 15 nm thick Ir film before the test. First, the electronic properties of thin Ir film are

studied to determine its Lorenz number. In the end, the thermal transport in DNA microfibers will be evaluated in detail.

3.2.1. DNA-promoted electron transport in Ir film on DNA microfiber

Figure 3.2(a) presents the electrical resistivity against temperature for two bulk Ir (data from Selbach[51] and White[52]) and for two Ir thin films in this work. The electrical resistivity of the Ir film is calculated out based on the measured electrical resistance, sample length, diameter, and the thickness of the Ir film. As shown in Fig. 3.2(a), the electrical resistivities of bulk Ir and Ir films are all proportional to the temperature at high temperatures (above 50 K). The rates of change of electrical resistivity with temperature ($d\rho/dT$) are identical. Below 50 K, the electrical resistivity starts to approach a certain value. This value is entitled "residual electrical resistivity" and is due to electron scattering by grain boundaries, static impurities and defects, which is essentially temperature independent. The residual electrical resistivities of the two Ir films are 2.20×10^{-7} Ωm and 3.22×10^{-7} Ωm, much higher than those of bulk Ir (almost zero). This is due to the increased electron scattering by the increased grain boundaries, impurities and defects when the Ir film is ultra-thin.[53]

The electrical resistivity can be decomposed as the sum of the residual electrical resistivity ρ_0 and the intrinsic electrical resistivity ρ_i as: $\rho_t = \rho_0 + \rho_i$. The intrinsic electrical resistivity is caused by thermal vibrations of lattice (phonons), and thus shows temperature dependent behavior. The shape of ρ_t~T plot is characterized by the Bloch-Grüneisen formula,

$$\rho_t = \rho_0 + \alpha_\rho \left(\frac{T}{\theta_R}\right)^5 \int_0^{\theta_R/T} \frac{x^5}{(e^x - 1)(1 - e^{-x})} dx, \qquad (3\text{-}2)$$

where α_ρ is a constant and θ_R is the Debye temperature. α_ρ is proportional to $\lambda_{tr}\omega_D/\omega_p^2$, where λ_{tr} is the electron-phonon coupling constant, ω_D is the Debye frequency, and ω_p is the Drude plasma frequency.[54]

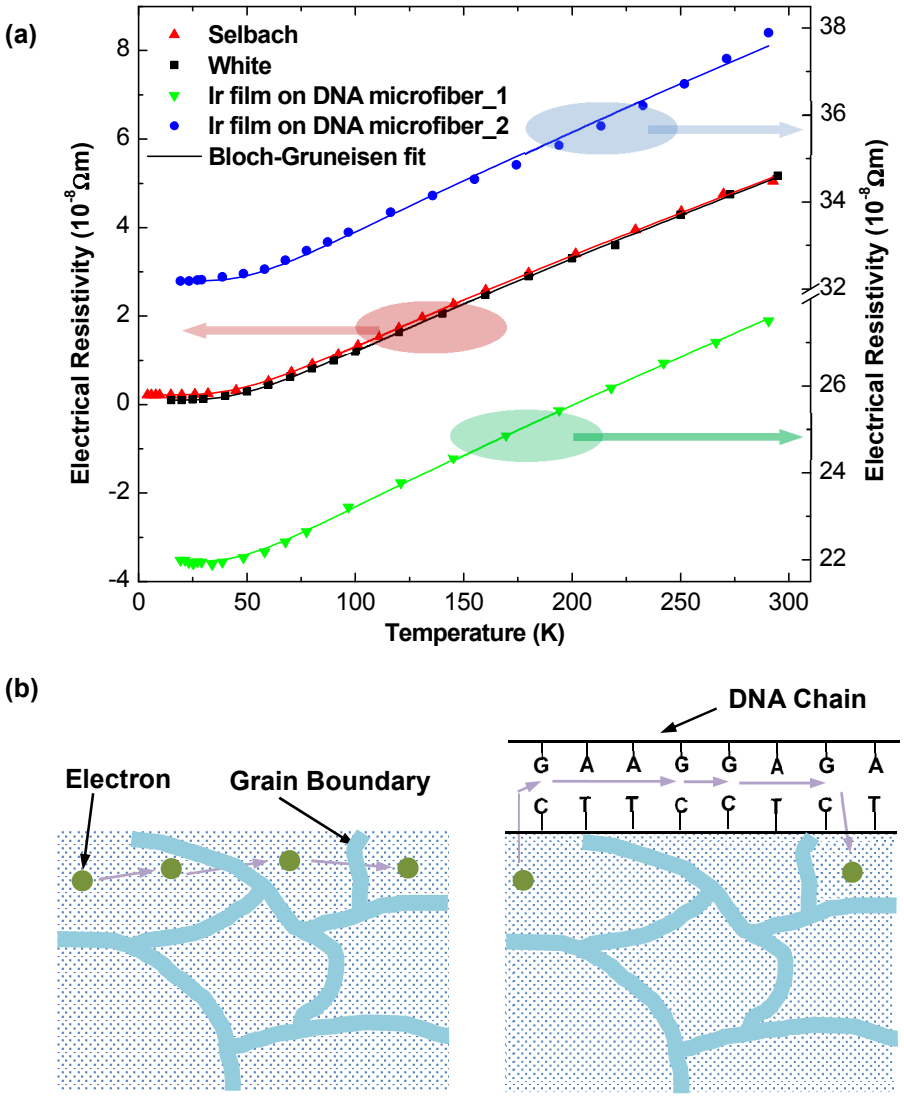

Figure 3.2. (a) Electrical resistivity of bulk Ir and nanoscale Ir film versus temperature. Solid curves are Bloch-Grüneisen fits. (b) Schematic of electron scattering from grain boundaries and electron transfer along DNA chains.

The solid lines in Fig. 3.2(a) are fits to the measurements by using Eq. (3-2). The

fitting has two parameters: α_ρ and θ_R. For two bulk Ir, the fitting results are: 21.86×10^{-8} Ωm and 22.34×10^{-8} Ωm for α_ρ, and 306.1 K and 307.6 K for θ_R. These values are consistent with each other. The Debye temperatures obtained are lower than the values extracted from the low temperature specific heat measurement (420K),[40] but close to the specific heat measurement made in the approximate range $\theta_R/2$ to θ_R, i.e. high-temperature value (290 K).[55] The fitting results for two Ir films on the DNA fiber sample are: 21.96×10^{-8} Ωm and 22.49×10^{-8} Ωm for α_ρ, 259.4 K and 285.9 K for θ_R. The Debye temperature values show a reduction by 7~15%. The reduction of Debye temperature is in agreement with previous studies on thin gold film,[53] as well as silver and copper nanowires.[56] This behavior is explained by phonon softening (more amorphous structures) at the grain boundaries in the thin metal film.[53, 57-58] The reduction of Debye temperature indicates a general reduction in frequency of the transversal-acoustic (TA) modes with respect to the corresponding modes of crystalline Ir. The reduction of the TA modes must be caused by decreased bond-bending forces in the amorphous structure. Nevertheless, the small reduction on Debye temperature has little effect on the intrinsic electrical resistivity. This is reflected by the fact that $d\rho/dT$ is identical for bulk Ir and Ir film at high temperatures, as shown in Fig. 3.2(a).

In above analysis, the intrinsic electrical resistivity of the nanoscale Ir film is found to be the same as bulk Ir. The identical electrical behavior against temperature seems expected, but it is not the case for Ir film on other materials, such as glass fiber, milk weed, and spider silk (data are not shown). At high temperatures (>50 K), $d\rho/dT$ for Ir film on these materials is around 1.0×10^{-10} Ωm/K, smaller than that for bulk Ir (2.1×10^{-10} Ωm/K). Then the fittings with the Block-Grüneisen formula are reexamined for these samples, and find that the fitted

parameters give similar θ_R but smaller α_ρ, with respect to the fitting results for Ir film on DNA microfibers. It is proposed that the electron scattering by grain boundaries in nanoscale Ir film is appreciable, which will indeed result in different electrical behaviors other than bulk Ir. However, DNA chains have the capability of transferring electrons over around ten nm by thermal hopping and quantum tunneling. This provides extra channels for electron transport other than through grain boundaries in the Ir film. The schematic of this physical process is shown in Fig. 3.2(b). The alternative paths of electrons preserve similar electrical behavior of Ir film on DNA fiber as bulk Ir. However, for other supporting materials, the electrons have no options but to transmit through the grain boundaries, leading to different electron conduction behavior. Since it is speculated that DNA chains provide extra channels for electron transport, the contact resistivity at the Ir-DNA interface is also speculated small to unblock the channels between Ir and DNA. However, at this point no evidence can be obtained on determining the contact resistivity. This could be important in future work to fully understand the electron transport mechanism in DNA-supported Ir film. In addition, the contact resistance is also speculated negligible due to large Ir coating area on supported DNA fiber.

3.2.2. Lorenz number determination for Ir film

3.2.2.1. Lorenz number determination at room temperature

For precisely estimating the Ir coating effect, the Lorenz number of Ir film L_{Ir} over a wide temperature range is needed. At room temperature, L_{Ir} is determined by the similar process as the Lorenz number determination for thin gold film described in Section 2.2.3. However, it is hard to keep the fiber structure unchanged during the cooling and heating

processes under reduced temperatures, and the sample constantly ends up with no resistance reading, indicating that the Ir film does not stay on the DNA microfiber continuously any more. As a result, the Lorenz number for Ir film is not able to be measured at reduced temperature. Nevertheless, with the Lorenz number precisely determined at room temperature, an expression of the Lorenz number as a function of temperature can be derived for the Ir film.

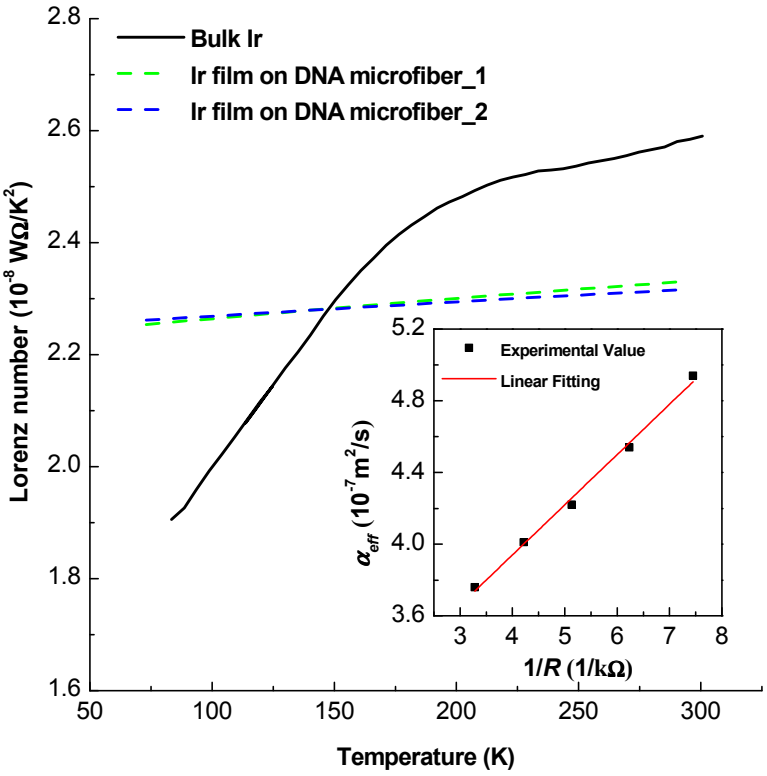

Figure 3.3. Variation of the Lorenz number with temperature for bulk Ir and Ir film on DNA microfibers. Inset: Linear fitting (solid line) of the effective thermal diffusivity (α_{eff}) against the electrical conductance ($1/R$) for Ir film on the DNA microfiber. The slope of the fitting line is determined as 2.8×10^{-5} $m^2\Omega/s$. Then the Lorenz number for Ir film on the DNA fiber is determined to be 2.38×10^{-8} $W\Omega/K^2$ at room temperature.

At room temperature, the DNA microfiber is first coated with a 15 nm-thick Ir film. Then another 5 nm-thick Ir film is coated on the top of the previous Ir film, and TET measurement is conducted to obtain α_{eff}. The same process is repeated until sufficient data are collected to do the fitting. In this case, the TET measurement is conducted with 20~40 nm Ir film with a step size of 5 nm. The α_{eff}~$1/R$ plot shown in the inset of Fig. 3.3 can be fitted with Eq. (2-12). The slope of the fitting line is determined as 2.8×10^{-5} $m^2\Omega/s$. With other known parameters, the Lorenz number for the Ir thin film on DNA microfiber is determined as 2.38×10^{-8} $W\Omega/K^2$ at room temperature. This value is close to the Lorenz number for bulk Ir, 2.58×10^{-8} $W\Omega/K^2$.[59]

3.2.2.2. Lorenz number at reduced temperatures

To determine the expression of Lorenz number as a function of temperature, we can start with the Wiedeman-Franz law,

$$L_{Ir} = \frac{\rho_t}{WT}, \tag{3-3}$$

where ρ_t is the electrical resistivity, and W is the thermal resistivity (inverse of the thermal conductivity κ_{el}). The thermal resistivity is $W = \kappa_{el}^{-1} = 3m_e / (\pi^2 n k_B{}^2 T\tau)$,[40] where m_e is the electron mass; n is the electron density; k_B is the Boltzmann constant; and τ is the relaxation time. Then a unified thermal resistivity can be defined as: $\Theta = WT$, which only changes with $1/\tau$ proportionally for the same metal. In this way, the unified thermal resistivity plays the same critical role as the electrical resistivity (also proportional to $1/\tau$) to reflect the electron scattering in metals.

Based on the electrical resistivity study, the intrinsic electric resistivity is observed to

be very close to that of bulk Ir. So it is physically reasonable to take the intrinsic unified thermal resistivity of Ir film the same as that for bulk Ir. Therefore, the Lorenz number for Ir film on DNA microfiber can be related to that for bulk Ir, as

$$L_{Ir} = \frac{\rho_{bulk} + \rho_e}{\Theta_{bulk} + \Theta_e} = \frac{\rho_{bulk} + \rho_e}{\Theta_{bulk} + \rho_e / L_e}, \tag{3-4}$$

where ρ_e, Θ_e are the extra residual electrical resistivity and extra residual unified thermal resistivity on top of bulk Ir, respectively, and $L_e = \rho_e/\Theta_e$. The only available electrical and thermal resistivity data extracted from the same bulk Ir sample is given in Ref.[60] The resistivity data are over an approximate temperature range of 80~300 K, not down to low temperatures. There is one advantage to deal with resistivity during this temperature range: both ρ_{bulk} and Θ_{bulk} are proportional to temperature. Thus, the resistivity data for bulk Ir in 80~300 K can be fitted as:

$$\rho_{bulk} = (0.02015T - 0.87711) \quad \times 10^{-8}\Omega\text{m} \tag{3-5-1}$$

$$\Theta_{bulk} = (0.00711T - 0.13977) \quad \text{mK}^2/\text{W}. \tag{3-5-2}$$

Note that the resistivity data will start to show non-linear characteristics for temperature below 80 K. Thus in general situations, Eqs. (3-5-1) and (3-5-2) are only valid to derive Lorenz number variation with temperature for Ir film in the temperature range of 80~300 K. For temperature below 80 K, these equations fail to capture the variation. The extra electrical residual resistivity (ρ_e) is the difference between the electrical resistivity of the Ir film and the electrical resistivity of bulk Ir at the same temperature. L_e is taken constant and is determined by the Lorenz number determination at room temperature. The measurement gives values of 6.83×10^{-8} Ωm for ρ_e and 3.05 mK^2/W for Θ_e. Thus, L_e is 2.28×10^{-8} $\text{W}\Omega/\text{K}^2$. Afterwards, Eq. (3-4) is used to evaluate the Lorenz number for Ir film at reduced temperatures. For example,

ρ_e for the Ir film on DNA fiber 1 is 22.53×10^{-8} Ωm at room temperature. Thus, the Lorenz number for this sample can be evaluated as

$$L_{Ir} = \frac{0.02015T - 0.87711 + 22.53}{0.00711T - 0.13977 + 9.8816} = \frac{0.02015T + 21.6545}{0.00711T + 9.7425} \quad \times 10^{-8}\,\mathrm{W\,\Omega/K^2}. \qquad (3\text{-}6)$$

Figure 3.3 shows the Lorenz number for Ir films and bulk Ir. It can be seen that the Lorenz number for the Ir films decreases with decreased temperature. However, the reduction is very small, only around 2%. The Lorenz number can be seen as constant over a wide temperature range. This is very different from the Lorenz number for bulk Ir, which has a larger reduction when temperature decreases. The difference stems from the fact that the large portion of residual resistivity in the resistivity for Ir film. Thus, the Lorenz number for Ir film is dominated by the static impurities, which has a constant Lorenz number independent of temperature. For temperatures below 80 K, the intrinsic resistivity becomes even smaller. Therefore, the Lorenz number of nanoscale Ir film is extrapolated to be a constant at lower temperatures.

3.2.3. Thermal transport in DNA microfiber

Two DNA microfibers are measured in the same manner down to 10 K. Here, DNA fiber 1 is discussed to show the data processing. The test temperatures are divided into three regions. For temperatures above 50 K, a linear correlation between temperature and resistance is adopted. With the sample size, dR/dT is interpreted as 1.733±0.019 Ω/K from Fig. 3.2(a). With dR/dT, the temperature rise due to the heating can be obtained based on the observed resistance increase. For example, at 190 K, the average resistance increase is 17.4 Ω. Thus, the temperature rise is found to be 10 K. As a result, k_{eff} is calculated as 0.44

W/m·K according to Eq. (2-7). Then the thermal conductivity of the DNA microfiber is obtained as 0.33 W/m·K by Eq. (3-1). α_{eff} is solved by fitting the normalized voltage increase to the theoretical solution shown in Eq. (2-9). The average α_{eff} at 190 K for this sample is 6.05×10^{-7} m^2/s. With k_{eff} and α_{eff}, ρc_p at 190 K is calculated to be 7.3×10^5 J/m^3K. The percentage uncertainty of ρc_p is ±6.11%. In the end, the thermal diffusivity of the DNA microfiber is obtained as 4.56×10^{-7} m^2/s. All results under temperatures above 50 K can be processed in the same way.

For temperatures between 20 K and 50 K, k_{eff} is not solved in the first place due to a large uncertainty in determining dR/dT. Instead, ρc_p at this temperature range are linearly extrapolated from the values obtained for the high temperature region [Fig. 3.4(c)]. α_{eff} is solved in the same manner as that for temperatures above 50 K. Then k_{eff} is obtained by multiplying α_{eff} with ρc_p. The thermal conductivity and diffusivity are obtained afterwards. For temperatures below 20 K, The sample needs to be heated till around 50 K to obtain a distinct TET signal. For such a wide temperature range, dR/dT cannot be considered constant. As a result, the TET technique is not applicable due to the strong non-linear signal. Therefore, the thermo-physical properties of DNA fiber 1 below 20 K are not extracted, though the electrical resistivity of Ir film is reported in that temperature range. The thermo-physical properties of DNA fiber 2 are reported down to 20 K for the same reason.

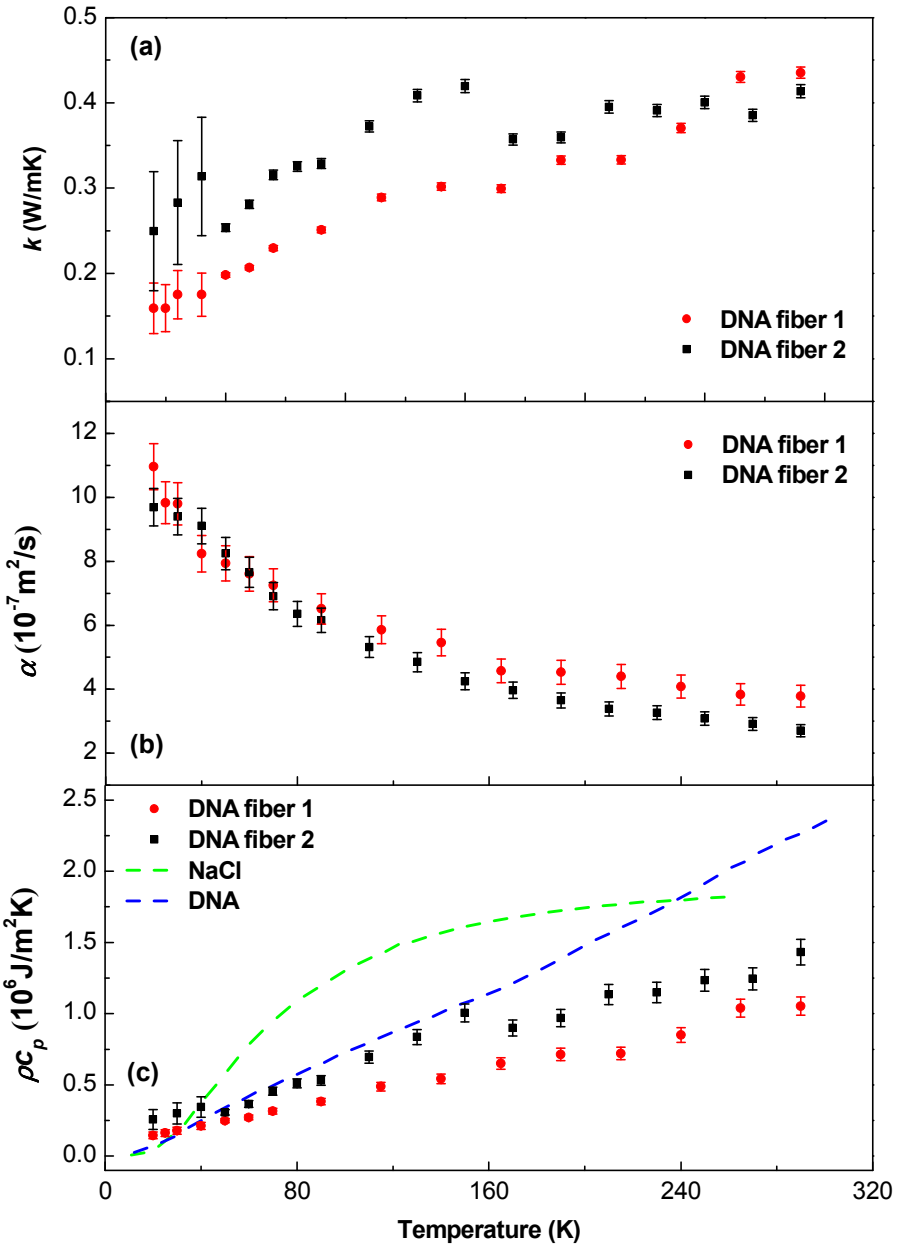

Figure 3.4. Temperature variations of thermal conductivity, thermal diffusivity, and volumetric heat capacity of DNA microfibers. The uncertainties are presented as error bars.

Temperature variations of thermal conductivity, thermal diffusivity, and volumetric heat capacity of DNA microfibers are shown in Fig. 3.4(a)~(c), respectively. The uncertainties of the measurements are presented as error bars. Two DNA microfibers have

similar results. At room temperature, the thermal conductivity is 0.42 W/m·K, close to the average result for the Group 2 fiber in Chapter 2 (Table 2.1, 0.33 W/m·K). As temperature goes down, the thermal conductivity gradually decreases. By contrast, the thermal diffusivity increases as temperature decreases. At room temperature, the thermal diffusivity is $3\sim4\times10^{-7}$ m/s^2. As temperature approaches 20 K, the thermal diffusivity increases to around $1\sim1.1\times10^{-6}$ m/s^2. The volumetric heat capacity of the DNA fiber is proportional to temperature, and approaches zero at low temperature. With an invariable density, the specific heat is implied to be proportional to temperature, in agreement with amorphous polyethylene[61] and native strands of Na-DNA.[62] Generally, the thermal conductivity of DNA fiber 1 is lower, and the thermal diffusivity of both fibers is similar. As a result, the volumetric heat capacity of DNA fiber 1 is lower. This can be explained by the reduction of density for DNA fiber 1 due to more pore structures.

With the temperature variations of thermo-physical properties for DNA microfibers, the following question can be answered: is the DNA microfiber crystalline DNA-NaCl composite or pure DNA bundle with negligible thermal effect from NaCl? The answer is pure DNA bundle. First of all, it is clear that NaCl crystallites are not observed in the SEM image [Fig. 3.1(a)]. To make a more persuasive conclusion, the temperature variations of thermo-physical properties of DNA fiber and NaCl[63] are compared. The thermal conductivity of NaCl increases with the decreasing temperature for high temperatures, and reaches the maximum value around 1000 W/mK at about 10 K. Then the thermal conductivity drops with the decreasing temperature. This variation is different from that of DNA microfiber, and the magnitude of thermal conductivity for NaCl is orders of magnitude higher. The variations of

thermal diffusivity are similar, but the magnitude for NaCl is 10~100 times larger. In the end, the volumetric heat capacities, whose magnitudes are in the same order, are compared. In Fig. 3.4(c), temperature dependence of the volumetric heat capacities of NaCl, DNA microfibers and native strands of Na-DNA[62] of salmon sperm are presented. The density of native strands of Na-DNA is chosen as 1.407×10^3 kg/m^3.[64] The heat capacity curve of NaCl is typical. At high temperatures, the heat capacity approaches a constant. At very low temperatures, the heat capacity obeys the famous Debye T^3 law. By contrast, the volumetric heat capacities of DNA microfibers and native strands of Na-DNA are proportional to temperature over temperatures up to 300 K. The reduction of volumetric heat capacity of DNA fibers than native DNA strands is also due to the reduction of density, as explained above. With all evidence, the DNA microfibers from Group 2 solution can be concluded to be DNA bundle, with negligible NaCl crystals.

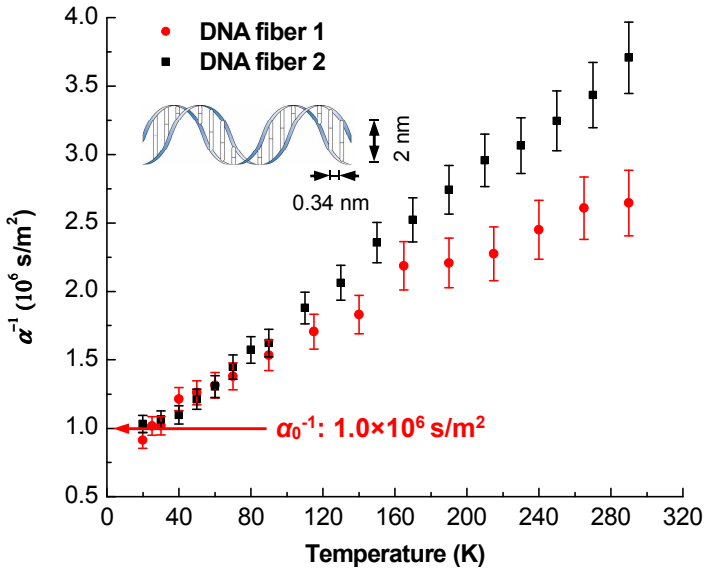

Figure 3.5. Temperature variation of thermal reffusivity for DNA microfibers. The residual thermal reffusivity is determined to be 1.0×10^6 s/m^2 for both fibers.

3.2.4. New defined parameter: thermal reffusivity

Under single relaxation time approximation, the phonon thermal conductivity κ_{ph} can be expressed as $\kappa_{ph} = Cv^2\tau/3$. Here C is the volumetric heat capacity (=ρc_p) and v is the average phonon speed which changes little with temperature. τ is the relaxation time. As the thermal diffusivity is defined as $\alpha = k/\rho c_p$, then $\alpha^{-1} = 3v^{-2}\tau^{-1}$. According to Matthiessen's rule, $\tau^{-1} = \tau_0^{-1} + \tau_U^{-1}$, where the subscripts "0" and "U" are for defect-induced scattering and phonon-phonon scattering (Umklapp processes). The defects include grain boundaries, point defects, disorders, and impurities. Thus, the inverse of thermal diffusivity can be written as the addition of residual part and intrinsic part, that is $\alpha^{-1} = \alpha_0^{-1} + \alpha_U^{-1}$. The inverse of phonon thermal diffusivity is introduced as a new parameter: thermal reffusivity. This parameter can be used to identify the thermal resistivity in DNA fiber that is caused by defect-induced scattering and by phonon-phonon scattering. Figure 3.5 shows the variation of thermal reffusivity with temperature for two DNA microfibers. It can be seen that α^{-1} increases almost linearly with increasing temperature. This is due to the fact that $\tau_U^{-1} \propto T$ since the phonon density increases almost linearly with temperature when the temperature is not very low. The thermal reffusivity theory is also examined on some bulk materials where phonons dominate the thermal transport process, such as silicon, germanium, and NaCl.[63] It is found that they all show very similar behavior as the DNA microfiber. The only difference is that α_0^{-1} is close to zero for these materials because the defects in them are very rare. At room temperature, α^{-1} is about 2.6×10^6 and 3.7×10^6 s/m^2 for the two DNA microfibers, respectively. The residual part: α_0^{-1} for both microfibers is around 1.0×10^6 s/m^2. This indicates that at room temperature the intrinsic thermal reffusivities are 1.6×10^6 and 2.7×10^6

s/m^2, respectively. Then the corresponding intrinsic thermal diffusivities of defect-free fibers can reach 6.3 and 3.7×10^{-7} m/s^2, 61% and 36% higher than the measured values. This is the prediction of the ultimate potential of the thermal diffusivity for DNA microfibers.

With the residual thermal reffusivity, the structural size for defect-induced phonon scattering l_0 can be determined. This parameter shows the average length that a phonon will be scattered by structural defects to lose its original energy information. The average sound velocity is estimated as $v = [1/(3v_L^3) + 2/(3v_T^3)]^{1/3}$, where v_L and v_T are the longitudinal and transverse sound velocities (3800 m/s and 3700 m/s in oriented DNA fiber respectively).[65] As a result, l_0 is 0.8 nm for DNA microfiber. This value is in the same order of characteristic sizes of DNA, which are 0.34 nm for one base pair length and 2 nm for DNA double helix width (inset of Fig. 3.5).[66]

CHAPTER 4. THERMAL TRANSPORT IN LAMBDA-DNA NANOFIBER

This work furthers the thermal transport study in DNA to the scale of DNA nanofiber. Compared to microfiber, DNA nanofiber has the great potential to possess a higher thermal conductivity since more oriented DNA and less structural defects are anticipated. In addition, testing nanoscale DNA samples is an essential to directly target its applications in nanoelectronics. In this work, λ-DNA is used for the thermal transport study. λ-DNA is 48,502 base pairs (bp) in length, longer than DNA from salmon testes (approximately 2000 bp). Given the same length in fabricating DNA fiber, λ-DNA fiber is expected to be thinner in diameter. Detailed study of a different type of DNA will also provide a broader understanding of thermal transport in DNA. In section 4.1, the preparations of λ-DNA nanofiber are described. The TET technique is modified to apply on nanoscale sample in Section 4.2. The thermo-physical properties of a λ-DNA nanofiber at 27~301 K are reported in Section 4.3 and 4.4.

4.1. Sample preparation

λ-DNA (48,502 bp, New England BioLabs) is diluted from 500 μg/mL to 50 μg/mL in TE buffer (10 mM Tris-HCl and 1.0 mM EDTA). The major differences between λ-DNA solution and salmon testes DNA solution are: the concentration of λ-DNA solution is 1% of the concentration for salmon testes DNA solution, and no NaCl is added in the λ-DNA solution. This completely eliminates any potential NaCl effect in DNA structure on phonon diffusion and scattering. The drawing of λ-DNA fiber is getting more difficult with a lower DNA concentration, due to less DNA molecules in the solution given the same volume of

droplet. Without NaCl, the negative charges on DNA molecules also prevent them to get close enough to form DNA bundle with a large diameter. To overcome the limitations, two strategies are developed: first the DNA droplet dropped onto the electrode within a fixed footprint is refilled a couple of times as it evaporates, in order to increase the concentration of DNA and extend the available pulling time; second the DNA fiber is drawn with a tungsten tip (tip diameter: 25 μm) controlled by a high-resolution 3-D micro-manipulator (525MT, Micromanipulator). The tip motion is well-controlled with a high motion resolution (0.7 μm) and stability. The entire drawing process is observed under an optical microscope. Once the DNA fiber is observed to be drawn out of the droplet on one electrode, it will move with the tip and attach to the second droplet on another electrode.

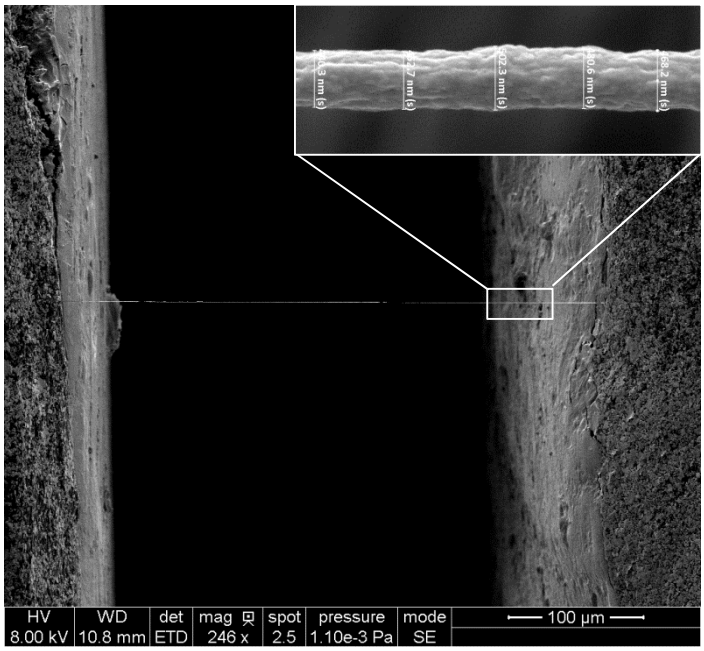

Figure 4.1. SEM image of λ-DNA nanofiber suspended between two electrodes for the measurement. Inset: Zoomed-in view of the λ-DNA nanofiber showing the diameter measurement.

The drawn λ-DNA nanofiber is suspended over the gap between the electrodes, as shown in Fig. 4.1. The λ-DNA nanofiber investigated in this work has dimensions of: 0.44 mm in length and 464 nm in diameter. The diameter of the λ-DNA nanofiber is less than one-tenth of that of average salmon testes DNA microfibers. The much smaller diameter size makes the surface-to-volume ratio of the nanofiber about one order of magnitude higher than the DNA microfibers. The great surface tension will facilitate significantly improved DNA alignment in the fiber, as discussed later.

4.2. TET characterization on λ-DNA nanofiber

The thermal transport study of λ-DNA nanofiber is carried out in the same cryogenic system as described in Chapter 3. The λ-DNA nanofiber is coated with a 50 nm gold film before the TET measurement. The gold film thickness is estimated from sputter time with the calibration of sputter rate.[67] Since the diameter of the λ-DNA nanofiber is comparable to the thickness of gold film, the cross-sectional ratio of the gold film χ cannot be approximated as 0. As a consequence, Eqs. (2-12) and (3-1) are not accurate to evaluate the thermal effect of gold film. Therefore, the regular TET technique needs to be modified to apply on nanoscale samples. The effective thermal conductivity measured in the TET technique is expressed as $k_{eff} = k_s + 8\varepsilon_r \sigma T_0^3 l^2 / 5D$, where k_s is the thermal conductivity of the gold-coated sample. k_s can be further decomposed as $k_s = k(1-\chi) + k_{Au}\chi$, where k is the thermal conductivity of the to-be-measured sample, and $k_{Au}\chi$ is the equivalent thermal effect of gold film. For microscale sample with $1-\chi \approx 1$, the thermal conductivity of the sample is obtained by Eq. (3-1). For nanoscale sample with $1-\chi \neq 1$, k has to be rewritten as

$$k = (k_{eff} - \frac{L_{Au} T_0 l}{R_0 A_e} - \frac{8\varepsilon_r \sigma T_0^3 l^2}{5D}) / (1-\chi). \quad (4\text{-}1)$$

Note that as $\chi \to 0$ for microscale sample, Eq. (4-1) can be simplified to Eq. (3-1). The measured effective thermal diffusivity α_{eff} can be used to determine the volumetric heat capacity of the sample: $(\rho c_p)_s = k_{eff} / \alpha_{eff}$. Then the volumetric heat capacity of λ-DNA nanofiber is obtained by $\rho c_p = [(\rho c_p)_s - (\rho c_p)_{Au} \chi] / (1-\chi)$. To the end, the thermal diffusivity of DNA is found through the definition: $\alpha = k / \rho c_p$.

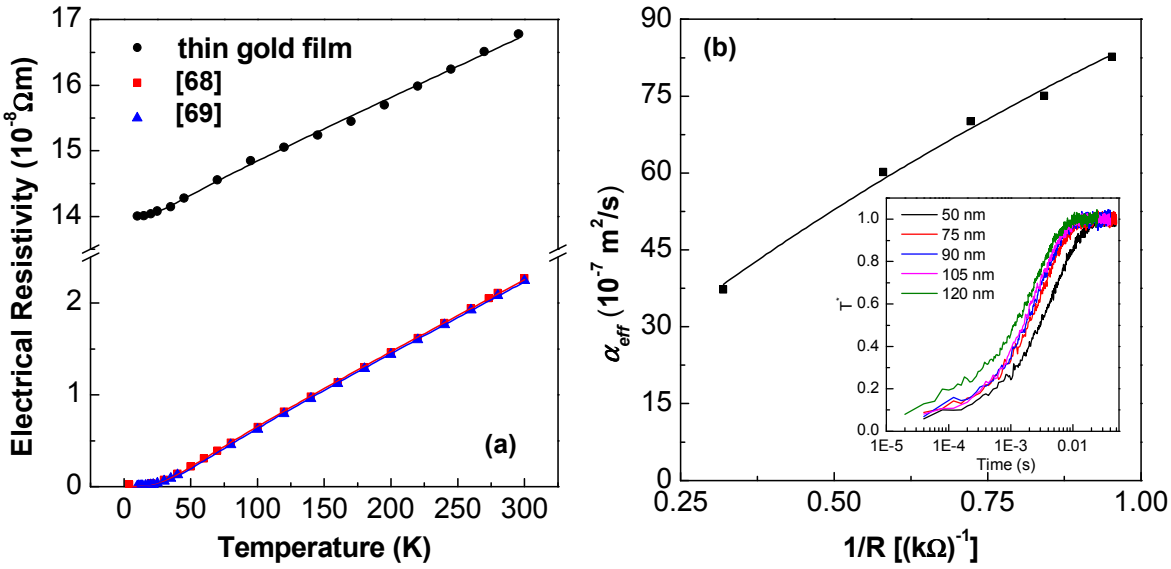

Figure 4.2. (a) Electrical resistivity for two bulk gold and thin gold film. Solid curves are Bloch-Grüneisen fits. (b) Fitting of α_{eff} against $1/R$ for Lorenz number determination at room temperature. Inset: normalized temperature increase T^* profiles by the TET technique with accumulated thickness of gold coatings. The T^* profiles are fitted to obtain α_{eff}.

To determine the Lorenz number of gold film on λ-DNA nanofiber, the electrical properties of the thin gold film are first studied. Figure 4.2(a) presents the electrical resistivity against temperature for two bulk gold[68-69] and thin gold film on λ-DNA nanofiber.

The electrical resistivity of the thin gold film is calculated out based on the measured electrical resistance, sample length, diameter, and the thickness of the gold film. The data can be fitted with Bloch-Grüneisen formula, shown in Eq. (3-2). For two bulk gold as references, the Debye temperature is found to be 168.3 K and 182.4 K, respectively. These values are close to the value extracted from specific heat measurement (170 K).[70] By contrast, the Debye temperature obtained for thin gold film is also reduced to 131.5 K, in agreement with Ir thin film on DNA microfiber. The reduction of Debye temperature is also explained by phonon softening. Meanwhile, the significant residual electrical resistivity ρ_0 in thin gold film is due to grain boundary and surface scatterings. As a result, the Lorenz number of thin gold film is dominated by the static scattering effects, which can be considered constant with respect to temperature. Therefore, the Lorenz number of thin gold film is to be determined at room temperature, and the obtained value is applied to the entire experimental temperature range afterwards.

The Lorenz number determination for thin gold film is conducted at room temperature by using the TET technique. The λ-DNA nanofiber coated with gold film measured in the cryogenic system is further processed for the Lorenz number determination at room temperature. The procedure is to measure the effective thermal diffusivity α_{eff} with accumulated gold coatings. First, the λ-DNA nanofiber coated with a 50 nm-thick gold film is measured by the TET technique. Then another 25 nm-thick gold film is coated on the top of the previous gold film, and the TET measurement is conducted again under the same experimental condition [inset of Fig. 4.2(b)]. Due to $\chi \neq 0$, the α_{eff} -1/R plot shown in Fig.

4.2(b) can be fitted by the following equation derived from Eq. (4-1) instead of using Eq. (2-12) directly,

$$\alpha_{eff} = \left[\frac{\pi D^2 k / 4 + L_{Au} l T_0 / R_0}{\pi D^2 / 4 + \rho_t l / R_0} + \frac{8 \varepsilon_r \sigma T^3 l^2}{5D} \right] / (\rho c_p)_s \qquad (4\text{-}2)$$

where ρ_t is the electrical resistivity for thin gold film. Note that Eq. (4-2) will be reduced to Eq. (2-12) as $\chi \to 0$. The fitting has two parameters: Lorenz number L_{Au} and thermal conductivity of λ-DNA nanofiber k. The fitting shows the Lorenz number for thin gold film is (2.43±0.08) $\times 10^{-8}$ WΩ/K^2, in agreement with bulk's value (2.35×10^{-8} WΩ/K^2 at 273 K and 2.40×10^{-8} WΩ/K^2 at 373 K) and thin gold film tested in Chapter 2 (2.27×10^{-8} WΩ/K^2). This value is then used to estimate the thermal effect of gold coating at all test temperatures.

The λ-DNA nanofiber is measured from room temperature to 10 K. The test temperature range is divided into two regions. For temperature above 20 K, a linear correlation between temperature and resistance is reasonably adopted to obtain dR/dT as 1.868±0.022 Ω/K. Then the temperature rise due to heating can be obtained based on the observed resistance increase. For example, at initial temperature T_0=95 K, the resistance increase due to heating is 25.13 Ω. So the steady temperature rise ΔT is estimated to be 13.45 K. As a result, $k_{eff} = q_0 l^2 / 12\Delta T = 2.57 \pm 0.24$ W/m·K. Then the thermal conductivity of λ-DNA nanofiber is 0.79±0.11 W/m·K from Eq. (4-1). This value is assigned to be the thermal conductivity at the average temperature during the heating, which is 101.7 K in this case. α_{eff} is solved by fitting the experimental normalized voltage evolution $V^*(t)$ with $T^*(t)$. Two data processing procedures are available for the fitting. In the first method, single-period raw data is directly fitted to theoretical predication, and the average value from multi-

period tests is taken as α_{eff}. Alternatively, the multi-period raw data can be first averaged to increase the signal to noise ratio before being fitted. Either way will give identical results. The percentage uncertainty of the fitting for latter data processing is estimated to be 5%. At T_0=95 K, α_{eff} is 3.39×10^{-6} m^2/s, so $(\rho c_p)_s$ is $(7.58\pm0.81)\times10^5$ J/m^3K and ρc_p is $(5.82\pm0.58)\times10^5$ J/m^3K, respectively. All results above 20 K are obtained in the same way. For T_0<20 K, dR/dT is not constant so that the non-linear effect is strong in the signal. As a result, thermo-physical properties of λ-DNA nanofiber below 20 K are not extracted, though the electrical resistivity/resistance of thin gold film is reported in this temperature range.

The thermal conductivity, volumetric heat capacity and thermal diffusivity of λ-DNA nanofiber at 27~301 K are plotted in Fig. 4.3(a)~(c) with error bars denoted as measurement uncertainty. At room temperature, the thermal conductivity is (0.94±0.21) W/m·K. As temperature decreases, the thermal conductivity first slightly increases and plateaued at 1.1 W/m·K till 126 K, and then reduces to 0.5~0.7 W/m·K at 27~50 K. By contrast, the volumetric heat capacity (specific heat) has a linear variation with temperature. The thermal diffusivity increases with decreasing temperature. The variations are in agreement with salmon testes DNA microfibers tested in Chapter 3.

The discovery is that the thermal conductivity of λ-DNA nanofiber is more than twice of DNA microfibers at almost any given temperature. At the molecular level, the thermal conductivity of λ-DNA nanofiber depends on its polymeric structure and in turn the value of thermal conductivity provides the information about DNA structure. The thermal conductivity is the product of two independent physical properties: volumetric heat capacity

and thermal diffusivity. Compared to DNA microfiber, the volumetric heat capacity and thermal diffusivity of λ-DNA nanofiber are both higher. First the λ-DNA nanofiber is concluded to contain less void structures because of its higher volumetric heat capacity. If the DNA is assumed to have a universal specific heat value, then possessing a higher volumetric heat capacity indicates that λ-DNA nanofiber has a higher density than microfibers. Using the specific heat data for DNA,[62] the density of λ-DNA nanofiber is estimated as 1073 kg/m^3, statistically larger than 901 kg/m^3 and 674 kg/m^3 for the two salmon testes DNA microfibers. The λ-DNA nanofiber is believed to be more condensed with a thinner structure, while the DNA microfiber may have more pore structures causing a lower density. Since the density of λ-DNA nanofiber is still lower than the density of dry DNA films (1407 kg/m^3)[64] and λ-DNA (1700 kg/m^3),[71] it is expected that there is still more room to increase the density if a fully condensed DNA nanofiber can be fabricated.

Second, it is speculated that the λ-DNA nanofiber contains more oriented DNA in the fiber's axial direction since the thermal diffusivity is much higher than that of DNA microfiber. It is found that the deformation-induced structural orientation will lead to increase of thermal conductivity/diffusivity while the volumetric heat capacity is not affected.[72-74] The stress-thermal rule is valid as that the thermal conductivity and stress tensors are linearly related. As the λ-DNA nanofiber is drawn from the solution, greater surface tension is imposed on the nanofiber than microfibers due to smaller surface-to-volume ratio. As a result, the deformation imposing on the λ-DNA nanofiber leads to more oriented DNA in the drawing direction, which in turn enhances the thermal conduction in the nanofiber.

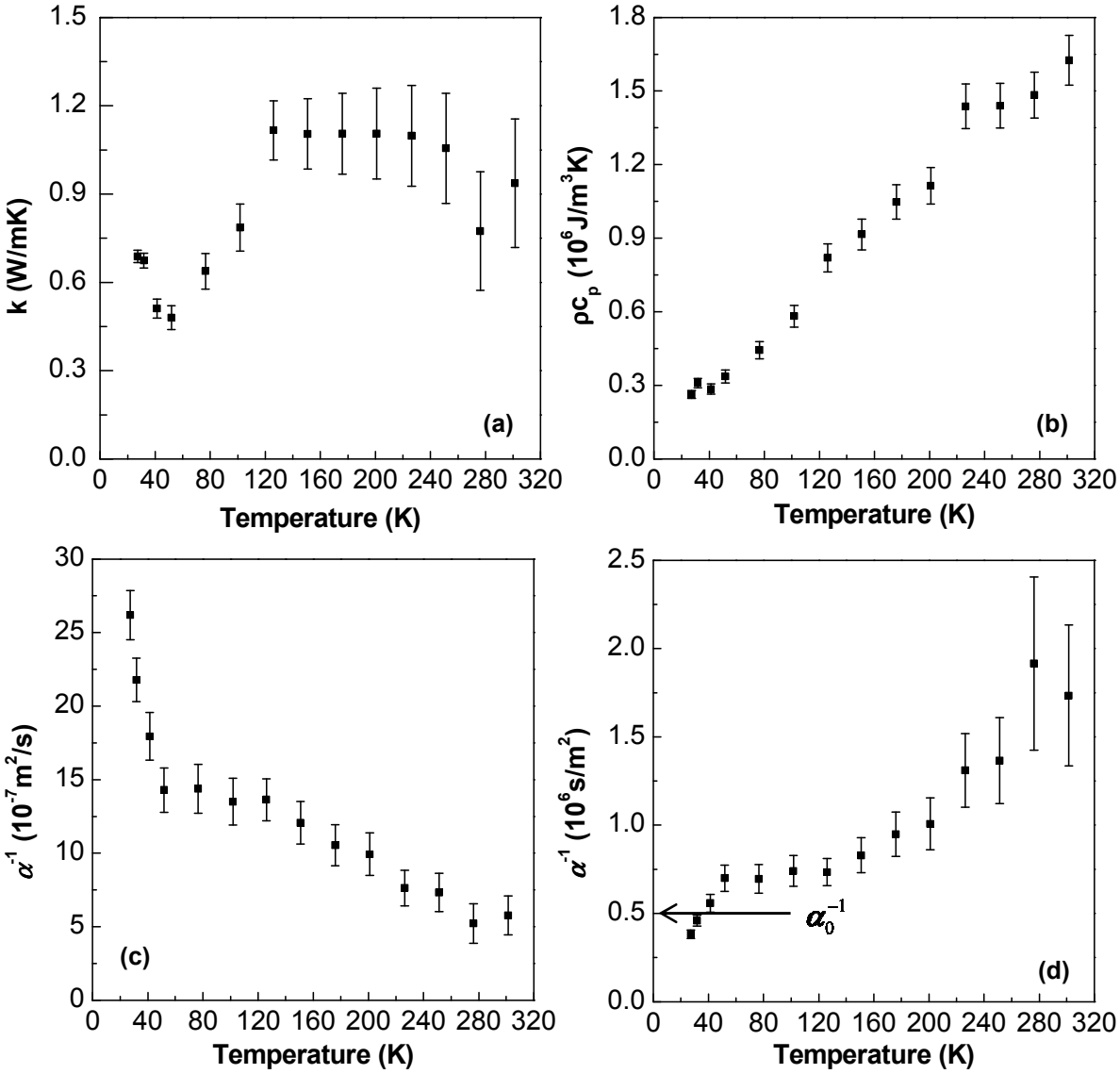

Figure 4.3. Temperature variations of (a) thermal conductivity, (b) volumetric heat capacity, (c) thermal diffusivity, and (d) thermal reffusivity of λ-DNA nanofiber. The uncertainties are presented as error bars. The residual thermal reffusivity is estimated to be 0.5×10^6 s/m^2.

4.3. Phonon diffusion length in DNA nanofiber

To further the study of thermal transport to the atomic level, the thermal reffusivity against temperature is plotted in Fig. 4.3(d). It can be seen that the thermal reffusivity α^{-1}

decreases with decreasing temperature. At 0 K limit, by extrapolating α^{-1} approaches the residual thermal reffusivity α_0^{-1}. In Chapter 4, the residual thermal reffusivity has been related with structural size of defect-induced scattering l_0 under single relaxation time approximation for all phonons: $\alpha_0^{-1} = 3/(vl_0)$, where v is the average phonon speed. However, the use of the approximation needs to be justified. Thus, here the thermal reffusivity theory is derived without using the single relaxation time approximation.

For any specific phonon with frequency ω and wave vector $\boldsymbol{k}$, its mean free path consists of the contributions from phonon-phonon scattering (Umklapp scattering: l_i, which is intrinsic to phonons and could vary with ω and $\boldsymbol{k}$) and defect-induced scattering mean free path (l_0) as $l^{-1} = l_0^{-1} + l_i^{-1}$. l_i is proportional to the inverse of phonon population. The average phonon number as the function of temperature is described by the Bose-Einstein distribution,

$$\langle n \rangle = \frac{1}{e^{\hbar\omega/k_B T} - 1} \tag{4-3}$$

where $\hbar$ is Planck's constant and k_B is Boltzmann's constant. $\langle n \rangle$ becomes very small when temperature goes to 0 K limit, indicating the phonon-phonon scattering is scarce and $l_i \to \infty$. So the defect-induced scattering is the only phonon scattering effect at 0 K limit, and phonons with different frequencies can be reasonably considered to share the same l_0 since only a few acoustic phonons with low frequencies are excited. Therefore the residual thermal reffusivity can be written as: $\alpha_0^{-1} = 3/(vl_0)$, As temperature goes up, l_0 could change since more phonons with higher frequencies are excited at higher temperature. However the change is expected to be small, the low temperature limit is meaningful as a very typical structure domain size for phonon diffusion. As seen in Fig. 4.3(d), $\alpha_0^{-1} \approx 0.5\times10^6$ s/m^2 for the

λ-DNA nanofiber. With an average phonon speed of 3734 m/s in DNA, l_0 is estimated as 1.6 nm. This size shows the average length that a phonon will be scattered by structural defects to lose its original energy information. Though it is not exactly equal to grain size since other defect effects also come into play, it is reasonable to estimate that the grain size is in the same order of l_0. In this case, the grain size is also in the same order of characteristic size of DNA. As speculated, the λ-DNA nanofiber contains more oriented DNA in the fiber's axis direction. So l_0 reflects the main structure size along the chain since the phonon diffusion is more likely along the DNA chain. In this case, l_0 is around 5-bp length for typical phonon scattering in the λ-DNA nanofiber. The size l_0 for λ-DNA nanofiber is twice of that for DNA microfibers (0.8 nm). The increase is partially due to less structural defects. In addition, the molecule orientation also increases the size for that the size obtained for DNA microfibers with less oriented structures is only a projection of the phonon diffusion length in the fiber's axial direction.

An infinite l_0 will indicate that there is no defect-induced scattering, and thus the thermal transport in DNA will be fully powered without defects. α_0^{-1} will be minimized to zero if this would happen, indicating that at room temperature the thermal reffusivity will be reduced to 1.23×10^6 m/s^2 for the defect-free λ-DNA nanofiber. Then the corresponding thermal diffusivity can reach 8.1×10^{-7} m/s^2, improved by 40% from the measured thermal diffusivity. In addition, if the volumetric heat capacity can also be maximized, the thermal conductivity for λ-DNA with perfect structure will reach 2.3 W/m·K at room temperature. This prediction is still only based on the very random base sequence in the λ-DNA studied in this work. If a DNA is built on one type of nucleotide, it will be more like a single crystal,

and the thermal conductivity will be significantly higher than 2.3 W/m·K.

CHAPTER 5. DNA NANOFIBER ARRAY FABRICATION AND THERMAL CHARACTERIZATION

In this Chapter, modified molecular combing approaches are developed to stretch DNA nanofibers with a diameter of around 100 nm or less to enable the thermal transport down to this scale. The DNA nanofiber array fabrication is introduced in Section 5.1, and the specificities of the TET technique employed for the thermal transport study on the DNA nanofiber between SU-8 micro-pillars are discussed in Section 5.2. The results are presented in Section 5.3, and the TET technique is developed accordingly to address the issues associated with current experimental setup.

5.1. DNA nanofiber array fabrication

A DNA molecule in aqueous solution is randomly structured at equilibrium. Entropy will shorten the distance between two ends of DNA chain to a much smaller size than the contour length. To investigate the thermal transport in DNA down to nanoscale, especially to the scale of 100 nm or less, it is essential to stretch DNA nanofibers from the solution over well-defined electrodes. In previous Chapters, the DNA molecules are stretched through drawing DNA micro/nanofibers by a tip from the solution. The thinnest DNA nanofiber is with a diameter of 464 nm shown in Chapter 4. However, all the other DNA fibers generated by this method have a diameter in microscale. Though polymers with a diameter as small as 130 nm are produced by using the similar method,[22] the chance of drawing nanofibers is highly related to the hands-on drawing experience. Alternatively, molecular combing is the simplest and most widely used approach to stretch and align DNA molecules.[75-81]

Conventionally, DNA molecule is stretched on either hydrophobic or hydrophilic substrates. Individual DNA molecule or bundle is stretched by a receding meniscus between the substrate and coverslip. Surface tension, acting perpendicular to the direction of motion of the meniscus, extends the DNA during movement. In molecular combing, DNA is strongly bound to the substrate with no chemical modification. However, conventional molecular combing is not applicable for this study. In the TET technique, the to-be-measured fiber needs to be suspended between two electrodes. In this way, heat can be conducted to the electrodes through DNA only. This is not a requirement for electrical conduction study as long as the substrate is electrically insulated.

Based on the molecular combing approach, modified methods are adopted to generate suspended DNA nanofiber array for thermal transport study. For the first method, DNA nanofiber array is generated on a poly (dimethyl siloxane) (PDMS) stamp containing micro-ridge patterns. In the second approach, DNA nanofiber array is generated to be suspended between superhydrophobic SU-8 micro-pillars.

5.1.1. DNA nanofiber array suspended on PDMS micro-ridges

The first approach is to generate highly ordered DNA nanofiber array through de-wetting of a DNA solution on a PDMS stamp containing micro-patterns.[21, 82-86] In this approach, DNA nanofibers are generated by placing a PDMS stamp on a small drop of aqueous DNA solution on a glass slide and then peeling it up. The drop will move relative to the PDMS stamp, and DNA nanofibers will be stretched and suspended between micro-patterns by the three phase contact line motion.[84]

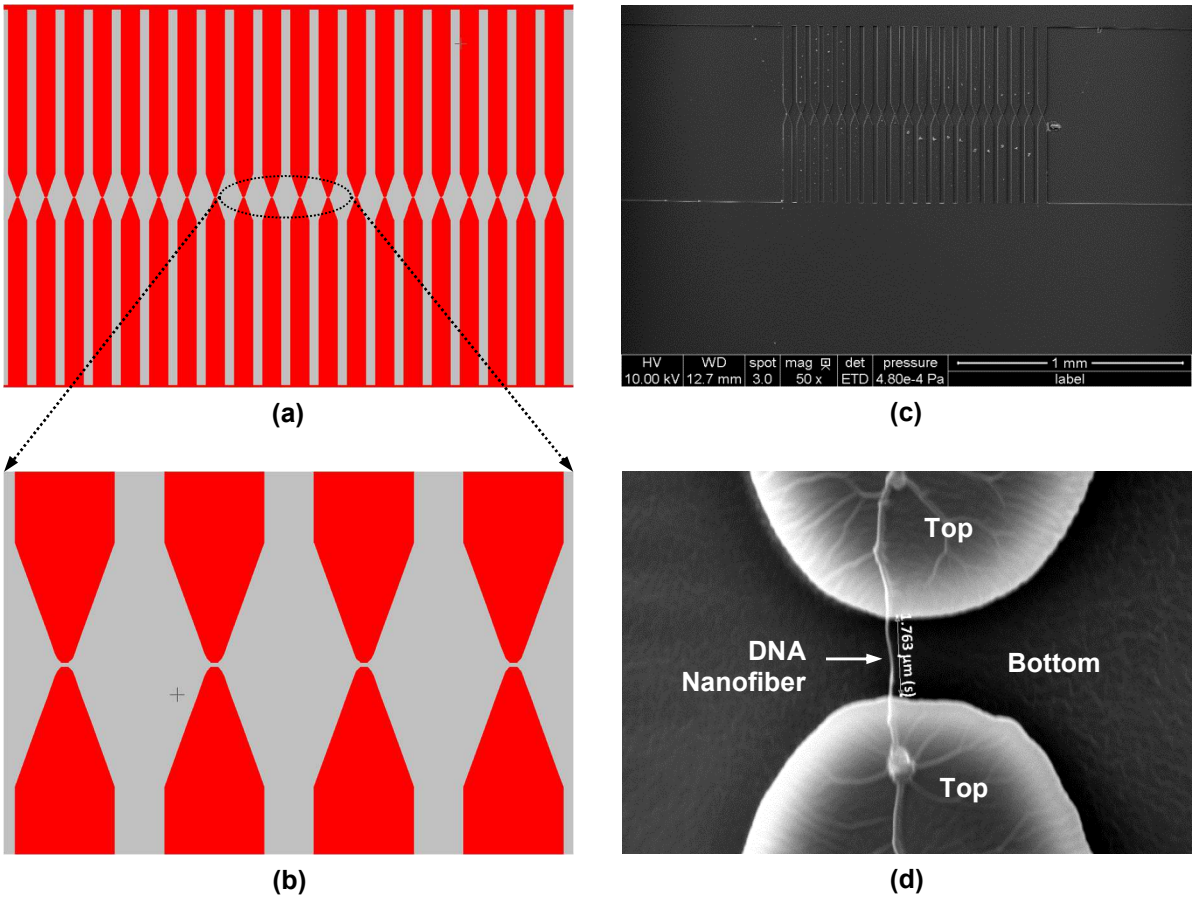

Figure 5.1. (a) Photomask design in L-Edit and (b) zoomed in view. (c) SEM image of PDMS stamp with micro-ridges after DNA nanofiber array fabrication. (d) One of the DNA nanofibers in the array stretched on PDMS stamp.

A design of the PDMS stamp with micro-ridge patterns, as shown in Fig. 5.1(a)~(b), is used to generate DNA nanofibers suspended across micro-ridges with ~2 μm separation. The first step is to fabricate a negative mold of the desired PDMS micro-patterns by standard photolithography techniques. L-Edit software is used to design the photomask for the photolithography fabrication of the mold. The photomask design and its zoomed view in L-Edit are shown in Fig. 5.1(a) and (b). Note that the red area represents chrome on the mask, i.e. unexposed area of the photoresist underneath the mask. The photoresist used is SU-8,

whose highly cross-linked structure will be formed under UV light exposure in the exposed area (grey area). As a result, the mold of SU-8 photoresist will be negative to the PDMS micro-ridge patterns. PDMS is then cast onto the SU-8 mold to produce a stamp with micro-ridges on the surface, which has the same geometry of the red area in Fig. 5.1(a) and (b). DNA nanofibers with a diameter of around 100 nm are successfully stretched on the PDMS stamp using this approach, as shown in Fig. 5.1(c) and (d).

After the fabrication of suspended DNA nanofiber array, the next step for the thermal characterization is to coat the sample with thin metal film to apply the TET technique. However, for the DNA nanofiber on PDMS stamp, one major issue during the metallization is that the thin metal layer on top of the micro-ridge is electrically connected to the bottom metal layer on the substrate. As a result, the metal-coated micro-ridges linked by a DNA nanofiber are not electrically insulated, resulting in the failure of the TET technique. This is confirmed by direct electrical measurement of metal-coated PDMS stamp without DNA nanofibers, which also shows conductive behavior between two micro-ridges. The failure of electrical insulation between the micro-ridges is probably due to the thin structure of the micro-ridges. The side walls of the micro-ridges are 4 μm high, which are limited by the thickness of SU-8 mold structure. As shown in Fig. 5.1, the negative SU-8 mold (grey area) has a smallest 2 μm width geometry feature, corresponding to the 2 μm separation between two micro-ridges. The geometry is much easier to collapse if SU-8 mold is too thick. As a result, the side walls of PDMS structure cannot be too thick. When depositing metal film on PDMS stamp, the side walls of the stamp will unavoidably be covered by some metallic atoms. This causes the electrical connection between the top and bottom metal layers.

5.1.2. DNA nanofiber array suspended on superhydrophobic SU-8 pillars

Another modified molecular combing approach is to generate suspended DNA nanofibers between SU-8 micro-pillars directly. By directly using SU-8, thick micro-pillars (~25 μm) can be fabricated. More importantly, the undercut sidewall feature of SU-8 further ensures sound electrical insulation[87] during the metal deposition, which is ideal for the TET technique (Fig. 5.2). This approach involves superhydrophobic substrate fabrication containing regular micro-patterns.[87-91] Same as the de-wetting method on PDMS stamp, controlled motion of the three phase contact line of DNA solution on superhydrophobic substrates enables the fabrication of suspended DNA nanofibers. The easiest way is to load a droplet of DNA solution onto a superhydrophobic substrate and dry.[92-94] Appropriate design of the geometry of micro-pillar patterns will enable the surface to be wetted in Cassie-Baxter mode,[94] in which the droplet stays on the top of micro-pillars without penetrating the spaces among them. As it evaporates, the three phase contact line will recede with time. Thus simple evaporation of the droplet will result in suspended DNA nanofibers with excellent radial orientation. Another way is to move the droplet on the superhydrophobic substrate, and the surface tension pushes DNA molecules to the surface and assists the combing and stretching of DNA molecules.[87, 95]

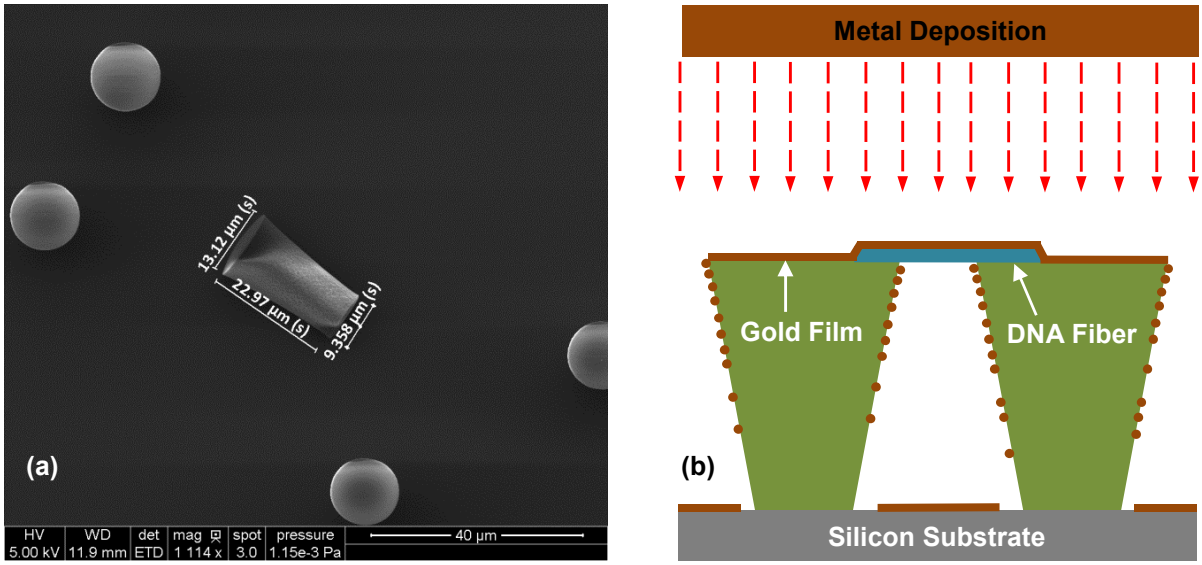

Figure 5.2. (a) The geometry of a collapsed pillar and its undercut sidewall profile. (b) Thick undercut SU-8 sidewalls enable the electrical insulation between pillars without DNA nanofiber and electrical connection with DNA nanofiber after metallization.

In this work, suspended DNA nanofibers have been generated on superhydrophobic substrate containing micro-pillar array by simply dropping the DNA solution onto the surface. The SU-8 pillar array is fabricated by using standard photolithography techniques. The pillar is designed as 15 µm in diameter and 25 µm in thickness. The geometry of a collapsed micro-pillar and its undercut sidewall profile can be seen in Fig. 5.2(a). The distances between the two nearest pillars are 10, 15, 20, and 25 µm for 4 pillar regions, respectively. The distance in this range will enable the droplet to stay on the top of pillars. For better adhesion of DNA nanofibers, the SU-8 surface is roughened by plasma nanotexturing treatment, and then a Teflon layer is deposited on the surface to increase hydrophobicity. The plasma nanotexturing is performed with inductively-coupled-plasma reactive-ion-etching (ICP-RIE, Plasmalab System 100, Oxford Instruments). The etching consists of a CF_4/O_2 flux (5/15

sccm) at pressure of 60 mTorr and an ICP/RF power of respectively 100 W and 50 W for 10 minutes. The Teflon deposition is achieved by taking the advantage of polymer deposition step of standard silicon etching in a deep trench etcher (SLR-770, Plasma-Therm). The deposition is processed for 10 s in a plasma environment created by in the injection of 85 sccm of C_4F_8 with a chamber pressure of 27 mTorr and an RF power of 600 W.

A drop of 5 μL λ-DNA in TE buffer solution is then loaded on the superhydrophobic substrate by using an Eppendorf tip and dried in ambient conditions. The drop has a high contact angle on the surface, indicating the superhydrophobicity [Fig. 5.3(a)]. The footprint of the drop gradually reduces when the contact line at the solid interface recedes with time. As a result, DNA nanofibers will be stretched and suspended on micro-pillars, as shown in Fig. 5.3(b). The drop will be finally attached to the substrate when it gets sufficiently small, and DNA nanofibers are stretched in radial orientation around the drop residue. The thinnest DNA nanofibers are found at farthest locations from the residue with a diameter of ~40 nm [Fig. 5.3(c) and (d)]. Since the linear polynucleotide chain of individual DNA molecule has a width of 2 nm, the generated DNA nanofibers are all composed of multiple stretched DNA molecules. The DNA fiber is getting thicker when it gets closer to the drop residue. This is expected since the solution concentration gets higher as it evaporates,[87] inducing thicker DNA fibers.

For the DNA nanofibers generated on SU-8 micro-pillars, the pillars are electrically isolated due to the thick undercut sidewall feature [Fig. 5.2(b)] after metal deposition (30~60

nm gold coating). As a result, the TET technique can be performed on the DNA nanofibers between SU-8 pillars.

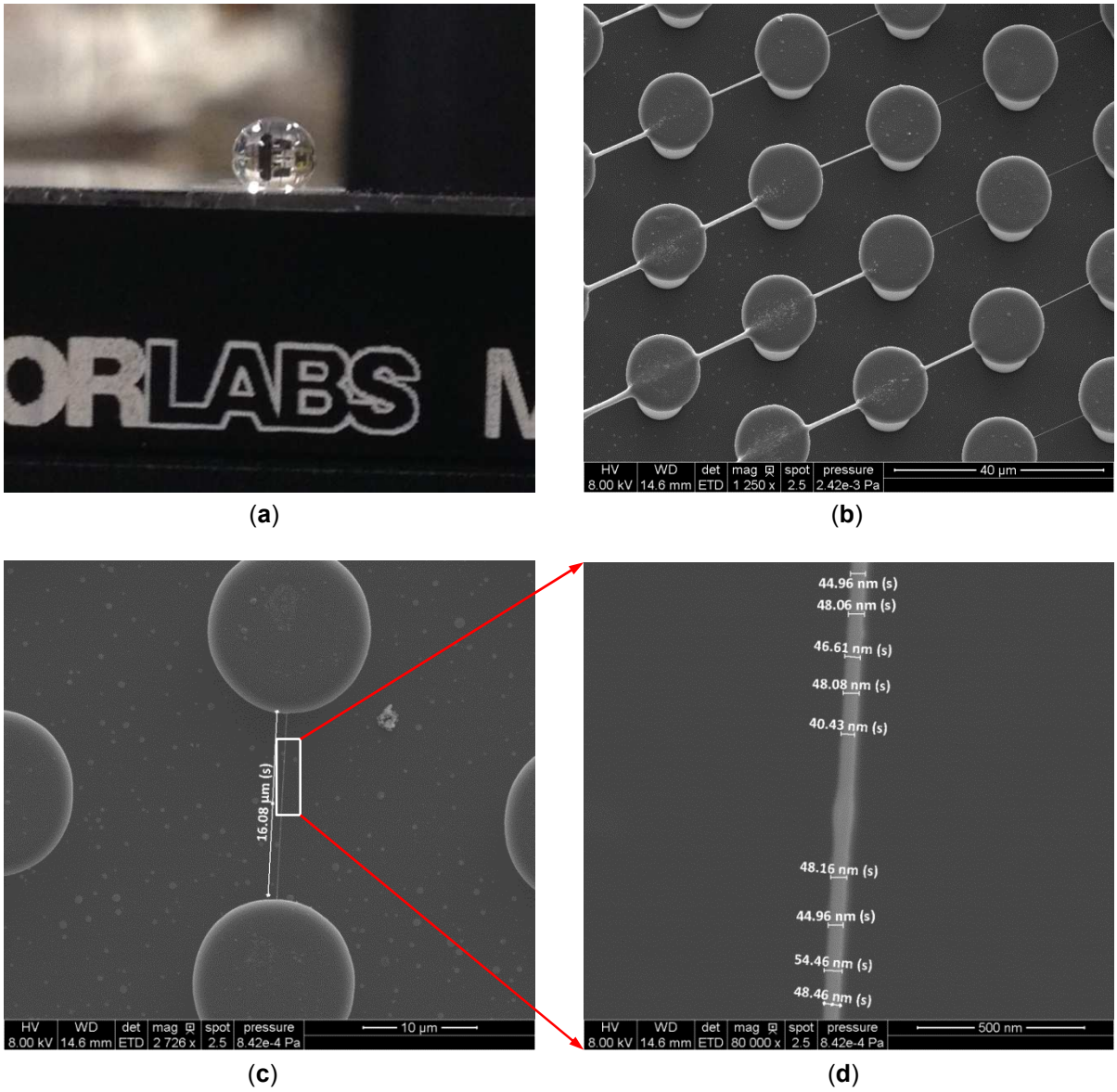

(**a**) (**b**)

(**c**) (**d**)

Figure 5.3. (a) A drop of DNA solution loaded on superhydrophobic substrate with high contact angle. (b) DNA nanofiber array suspended on the SU-8 micro-pillars. (c)~(d) Thinnest DNA fiber with a diameter of ~40 nm found at the farthest locations from the DNA drop residue.

5.2. Thermal characterization on DNA nanofiber between SU-8 pillars

The TET characterization on DNA nanofiber fabricated between SU-8 pillars has its own specificities. First, the radiation effect in the expression of effective thermal diffusivity shown in the Eq. (2-12) is estimated as 1.6×10^{-10} m^2/s, orders of magnitude smaller than the estimated effective thermal diffusivity of the DNA nanofiber sample ($\sim10^{-6}$ m^2/s). The radiation effect is proportional to the dimensional size: l^2/D. The length of DNA nanofiber between micro-pillars is in a range of 10~25 μm, an order of magnitude smaller than the DNA micro/nanofibers studied in previous Chapters. As the sample size shrinks, the radiation effect becomes negligible. Second, the characteristic rise time in the TET technique becomes extremely short. The characteristic rise time can be estimated as $\Delta t_c = 0.2026 l^2 / \alpha_{eff}$.[25] If the effective thermal diffusivity α_{eff} is assumed to be around 10^{-6} m^2/s, Δt_c is estimated as 20.3 μs for a DNA nanofiber with 10 μm long. For such a short characteristic time, the current source used in the TET technique has to be with a much faster rise time. The current source (6221, Keithley) used in this work has a typical rise time of 2~4 μs when the loading current is larger than 2 μA. Thus, the instrument rise time is still faster, which enables the application of the TET technique on DNA nanofiber between SU-8 pillars. To further improve the instrument rise time, the current source used for heating the sample can be replaced by a diode laser (UltraLasers, Inc. MSL-III-532-AOM-150 MW) modulated by a function generator (DS345, Stanford Research Systems) with a square wave function output. The nominal rise time for the function generator is less than 15 ns, orders of magnitude shorter than the sample's characteristic rise time. Third, due to the gold-covered pillar with a small surface area served as the electrode, the TET characterization has to be

performed on a probe station equipped with micromanipulators (525MT, Micromanipulator). The micromanipulators are used with tungsten probes (tip radius 5 μm, 7D, Micromanipulator) for contacting the pillars, as sketched in Fig. 5.4(a). Since the probe station is set up in standard laboratory conditions, the TET characterization has to be performed with surrounding air. This may introduce heat convection and conduction by air in the TET characterization and will be discussed later.

5.3. Results and discussion

5.3.1. Instrument rise time vs. characteristic rise time

Multi-period raw data are first averaged manually to increase the signal to noise ratio and a typical *V-t* profile for the TET technique on DNA nanofiber (640 nm in diameter, ~11 μm long) is shown in Fig. 5.4(b). Unlike the *V-t* profile shown in previous Chapters, the response of the current source as a second-order system is coupled with the regular TET voltage rise profile. The instrument rise time is estimated as 2 μs from Fig. 5.4(b), in agreement with the nominal value stated before. However, the characteristic rise time of the TET voltage rise profile is only about 4~5 μs, much shorter than the estimated value (~20 μs). This makes the starting point as the initial voltage indistinguishable and the TET technique inapplicable to this sample. The short rise time implies the effective thermal diffusivity is much higher than 10^{-6} m^2/s. One probability is that the thermal diffusivity of DNA nanofiber is very high, or the thermal transport to air environment is significant. As a result, two strategies have to be applied: first the current source is replaced by a diode laser modulated by a function generator with a square wave output, in order to further improve the instrument rise time. Second the thermal effect of air has to be estimated.

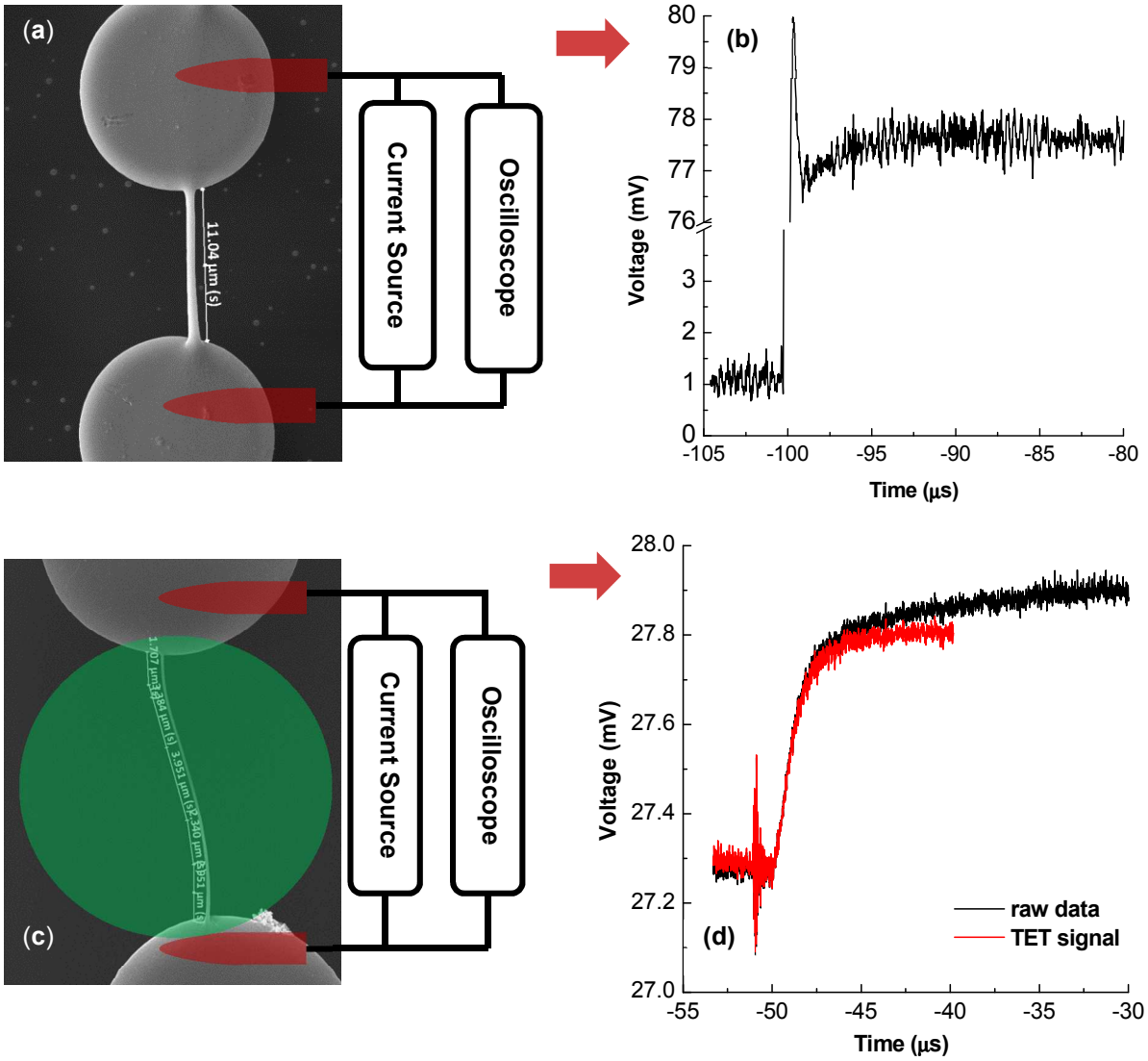

Figure 5.4. (a) Schematic of the experimental setup for the TET technique with a tungsten probe on DNA nanofiber between SU-8 pillars. (b) Typical *V*-*t* profile for the TET technique applying on the DNA nanofiber. (c) Schematic of the experimental setup for the TET technique with laser heating. The current source still provides a small dc current as probing current. The laser beam is sketched as green circle and the actual size should be much larger. (d) Typical *V*-*t* profile and intrinsic TET signal for the developed TET technique with a laser heating source on DNA nanofiber.

The laser beam is directed to the microscope (Olympus BX51) adapter through a collimator, and is focused on the sample surface within an area with a diameter of ~50 μm, as sketched with a circle in Fig. 5.4(c) (the actual size should be larger). The laser power is adjusted by a variable optical density filter. In this case, the laser power is reduced to 10% of the maximum. Figure 5.4(d) shows the *V*-*t* profile with laser heating for a DNA nanofiber (16.1 μm long, 150 nm in diameter). The current source still provides a small dc current as a probing current. The starting point of the voltage rise profile is captured with a trigger source from the function generator and the profile is collected in an average mode (512). As expected, the instrument rise time is negligible. But the voltage seems not to stay steady at the steady state. This is due to that the laser beam also heats the whole area besides DNA nanofiber, making the ambient temperature increases slowly. However, the time scale for this heating effect is much longer than the characteristic rise time in the TET signal, and its effect is not significant within the transient phase of the TET signal. The quasi-steady region is linearly fitted and subtracted to obtain the true steady state voltage, as shown in Fig. 5.4(d). The transient phase of the TET signal stays the same, which confirms that the overall heating has little impact on the TET signal. Now the experimental data are ready to do the fitting. Without considering the air conduction and convection effects, the effective thermal diffusivity of the sample is 2.13×10^{-5} m^2/s. The thermal diffusivity of DNA nanofiber is obtained to be 2.2×10^{-5} m^2/s after excluding the gold coating effect, two orders of magnitude larger than the value obtained in Chapter 4. Though the enhancement of thermal conduction in DNA nanofiber is expected as the diameter becomes smaller, it is speculated that the air conduction and convection effects are also significant. To estimate the heat conduction from

nanofiber to air environment, a two-layer theory for rarefies gas heat conduction is introduced. Simulation results of the TET technique with heat conduction to air environment are shown afterwards.

5.3.2. Thermal transport to the air environment

The Knudsen number *Kn*, in this case, is defined as the ratio between the mean free path of air molecules (l_m) and the diameter of the DNA nanofiber (D) to exhibit the gas rarefaction. In the non-continuum region with $Kn>10$, the free molecule theory should be used and the Fourier law is not valid. By contrast, in the continuum regime with $Kn<0.01$, the Fourier law and the continuum approximation are valid. The mean free path of air is estimated as 145.8 nm by $l_m = 3k_a / (\rho c_p v)$, where k_a and ρc_p are the thermal conductivity and volumetric heat capacity of air. $v = \sqrt{2k_B T / m}$ is the average speed of air molecules at temperature T, where k_B is Boltzmann's constant and m is mass of an air molecule. For the DNA nanofiber with a diameter of 150 nm [Fig. 5.4(c)], *Kn* is around 1. This indicates that the heat transfer between the DNA nanofiber and air can neither be described by the continuum approximation nor by the free molecular theory. As a result, a two-layer theory[96-97] is developed to investigate the thermal transport from nanofiber to the air environment in this region. The inner layer is non-continuum region with a thickness of molecular mean free path, and the outer layer is continuum region. In addition, the natural convection is ignored due to the buoyancy force is far less than the viscous force when the sample's diameter is smaller than 1 μm.

In the non-continuum region, the dissipated power $Q_{w\to nc}$ at the fiber surface can be described as

$$Q_{w\to nc} = \pi Dl \cdot \frac{A}{6} \cdot \rho c_p v (T_w - T_{nc}), \tag{5-1}$$

where l is fiber length, T_w is the fiber temperature, T_{nc} is temperature of the inner layer, and A is the parameter to be determined. In the continuum region, the dissipated power $Q_{nc\to\infty}$ is

$$Q_{nc\to\infty} = \frac{2\pi l k_a}{\ln \frac{r_2}{D/2 + l_m}} (T_{nc} - T_\infty), \tag{5-2}$$

where r_2 is radius at temperature T_∞. With $Q_{w\to nc} = Q_{nc\to\infty}$, the parameter A can be expressed as:

$$A = \frac{6}{[\Delta T / Q - (\ln \frac{r_2}{D/2 + l_m}) / (2\pi l k_a)] \pi dl \rho c_p v}. \tag{5-3}$$

Experimental data used to determine A are from Ref:[98] D=0.15 mm, l=97 mm, c_p=1005 J/kgK, v=446.85 m/s, ΔT=50 K, k_a=0.0263 W/m·K, and r_2 = 50 mm. The density and molecular mean free path l_m of air at normal pressure are 1.205 kg/m^3 and 145.8 nm, so $l_m = 1.47\times10^{-4} / P(\text{mBar})$ and $\rho = 1.19\times10^{-3} P(\text{mBar})$ when the ideal gas assumption holds. As a result, A can be expressed as a function of P and Q. Then A is found to be 0.8 for Kn~1 from the P~Q plot shown in the Fig. 6 of Ref.[98] As a result, the effective thermal conductivity λ' for the rarefied air layer can be expressed as

$$\lambda' = \frac{DA\rho c_p v \ln(1 + 2K_n)}{12}. \tag{5-4}$$

λ' is estimated as 0.0051 W/m·K for the DNA nanofiber shown in Fig. 5.4(c), 22.2% of that for air. Afterwards, the heat transfer process in the TET technique with additional thermal conduction from DNA nanofiber to air environment can be modeled by Fluent.

5.3.3. Simulation results by Fluent

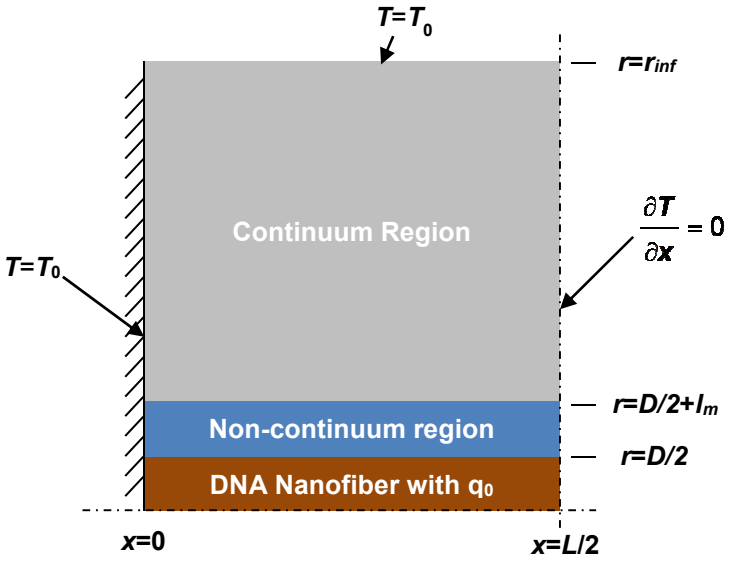

Figure 5.5. Schematic of computational domain and boundary conditions for the heat transfer problem from DNA nanofiber to the air environment.

The schematic of computational domain and boundary conditions for the simulations are shown in Fig. 5.5. The transient thermal transport process is modeled by Fluent 15.0. The computations are calculated with a time step size of 2 ns. The temperature along the axis of the DNA nanofiber is averaged for each time step. In this way, the computational temperature rise profile can be obtained. Though the electrical heating power per volume q_0 is just an estimated value in the simulation, it has no effect on the normalized temperature rise profile. In each case, a normalized temperature rise profile can be computed with a

specific thermal conductivity of the nanofiber. By varying the thermal conductivity, normalized temperature rise profiles can be plotted and compared with the experimental normalized voltage profile, as shown in Fig. 5.6. The best fit is with k=10 W/m·K. The effective thermal conductivity of the DNA sample has been largely reduced from the regular TET fitting results (~43 W/m·K). This result shows that the thermal conduction by air is significant. After excluding the gold effect by using Eq. (4-1), the thermal conductivity of DNA nanofiber is 2.5 W/m·K. However, this study finds relatively large uncertainty in calculating the thermal conductivity of DNA nanofiber, due to the fact that the thermal conduction from the sample to air environment is significant in the experiment. To reduce the uncertainty, the experiment has to be conducted in a vacuum chamber to fully exclude the air effect in future work.

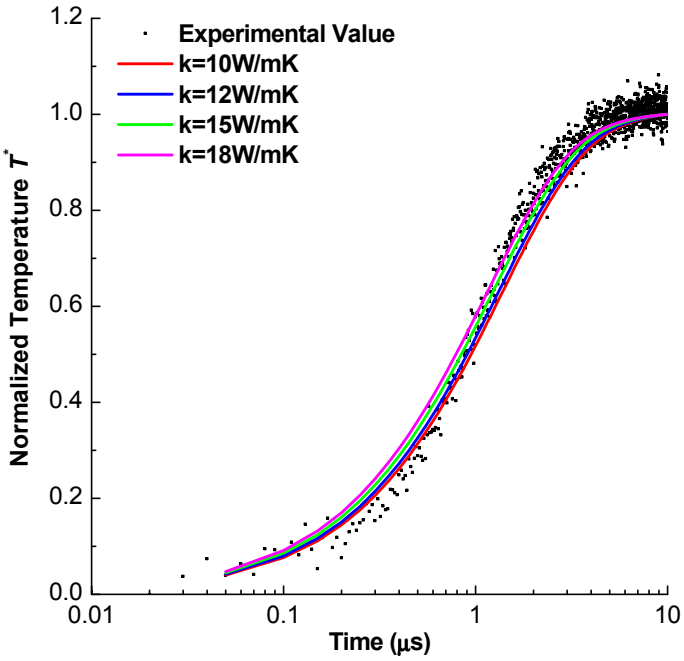

Figure 5.6. Comparisons between simulations and experimental result.

5.3.4. Electrical contact resistance

One more issue that has not been addressed in the thermal characterization is the electrical contact resistance. In previous Chapters, the DNA micro/nanofibers are connected to large electrodes by applying silver paste. The electrical contact resistance is estimated only a few ohms and thus is ignored. In this work, the electrodes are made of SU-8 pillars coated with 30-nm gold film, the electrical contact resistance between the gold film and tungsten tip need to be justified. The electrical contact resistance can be assumed to be the same for the DNA nanofibers on the same SU-8 pillar array, since the pillar array carrying with DNA nanofibers are coated with gold film all together. The measured electrical resistance R_t is the sum of electrical contact resistance and resistance of the gold-coated sample as: $R_t = R_c + R_0$, where R_c is electrical contact resistance and R_0 is the sample's resistance. Thus, the measured electrical resistance can be written as:

$$R_t = R_c + \rho_t \frac{l}{Dt}, \tag{5-5}$$

where ρ_t is the electrical resistivity of gold film, l is sample's length, D is sample's diameter and t is the thickness of gold film. Thus, for the DNA nanofibers on the same pillar array, the measured electrical resistance can be plotted as the function of l/D, as shown in Fig. 5.7. The contact resistance is extrapolated as 140 Ω. As a result, the real electrical resistance of the sample is reduced to 544 Ω for the DNA nanofiber shown in Fig. 5.4(c). After correcting the electrical resistance, the thermal conductivity of the DNA nanofiber is 0.6 W/ m·K. The result is in the same order of DNA nanofiber with a diameter of 464 nm, as well as those of DNA microfibers.

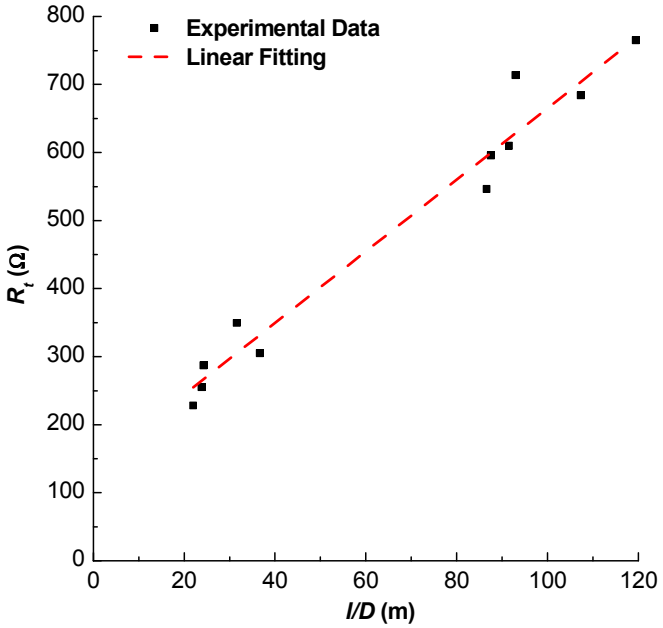

Figure 5.7. Measured electrical resistance versus the dimensional size l/D. The electrical contact resistance is extrapolated as 140 Ω.

CHAPTER 6. CONCLUSION AND FUTURE WORK

6.1. Conclusion

6.1.1. Conclusion on thermal transport in crystalline DNA micro-composites

In this work, crystalline DNA-composited microfibers and microfilms were synthesized, and their thermal transport capacities were characterized. The DNA micro-composites were formed from two groups of solutions: Group 1 is 0.5 wt% salmon testes DNA with 5 wt% NaCl, and Group 2 is 1 wt% salmon testes DNA with 1 wt% NaCl. The formation of crystalline DNA-NaCl complexes was speculated to align the DNA molecule with the crystal structure of NaCl during crystallization, which resulted in a significant enhancement of thermal transport within the composites, including both fibers and films. The films were found to have a higher capacity of thermal transport than the fibers, largely due to a higher degree of crystallization as well as more contributions from NaCl in terms of thermal transport. The thermal conductivity of DNA microfiber was speculated to be 0.33 W/m·K, which was concluded from the results for Group 2 microfibers who had least thermal effect from NaCl.

6.1.2. Conclusion on energy transport in DNA microfiber down to 10 K

In this work, electron transport in nanometer-thick Ir film supported by DNA microfiber fabricated from Group 2 solution and the phonon transport sustained by the DNA itself were extensively studied under low temperatures. Compared to bulk Ir, Ir film on DNA microfiber had a similar intrinsic electrical resistivity but a much larger residual electrical resistivity. The Debye temperature of Ir film showed a small reduction (7~15%) from bulk Ir,

which was explained by phonon softening. The similar intrinsic electrical resistivity was speculated to be preserved by the coherent quantum tunneling and diffusive thermal hopping effects for electron transport in DNA, which provided extra channels for electron transport other than through grain boundaries in the Ir film. The large residual electrical resistivity was due to the increased electron scatterings by the increased grain boundaries, impurities and defects in the Ir film. With the electrical resistivity study, the Lorenz number of Ir film was found to be unchanged over a wide temperature range due to the static impurities and the Lorenz number of Ir film was evaluated to be close to that of bulk Ir at room temperature.

Temperature variations of the thermo-physical properties of DNA microfiber confirmed that the DNA microfiber generated from Group 2 solution was a DNA bundle with negligible thermal effect from NaCl crystals. A new parameter, entitled “thermal reffusivity”, was defined to quantitatively determine the impact of structural defects on phonon scattering, and was widely used to predict the phonon thermal transport potential of defect-free materials. For the DNA microfiber, the thermal conductivity/diffusivity could be promoted by 36~61% if the residual thermal reffusivity caused by structural defects became zero. The structural size for defect-induced phonon scattering is estimated to be 0.8 nm in DNA microfiber.

6.1.3. Conclusions on energy transport in λ-DNA nanofiber

In this work, thermo-physical properties for a λ-DNA nanofiber were reported at 27~301 K. The λ-DNA nanofiber was found to possess a thermal conductivity of 0.94 W/m·K at room temperature, much higher than that of DNA microfiber. At almost any given

temperature, the thermal conductivity of λ-DNA nanofiber was more than twice of that for DNA microfiber. The enhancement of thermal conduction was due to more condensed and oriented structures and less structural defects. The more condensed structure was reflected by a higher density value. The more oriented DNA structures and less structural defects were concluded from a higher thermal diffusivity and a lower residual thermal reffusivity, which were the major origins of the enhancement of thermal conduction in the λ-DNA nanofiber. The structural size for defect-induced phonon scattering in λ-DNA nanofiber was 1.6 nm, twice of that in DNA microfiber. The increase was partially due to less structural defects. In addition, the molecule orientation also increased the size for that the size obtained for DNA microfibers with less oriented structures was only a projection of the phonon diffusion length in the fiber's axial direction. Since the λ-DNA nanofiber contained more oriented DNA in the fiber's axis direction, the structural size reflected on the main structure was more likely along the DNA chain. In this case, the size was around 5-bp along λ-DNA nanofiber. As the structural size approached to infinity, the defect-induced phonon scattering could be eliminated. As a result, the thermal conductivity for λ-DNA with perfect structure was predicted to be 2.3 W/m·K at room temperature.

6.1.4. Conclusions on thermal characterization of DNA nanofiber array

In this work, DNA nanofiber array was fabricated for the thermal transport study. Highly ordered DNA nanofiber arrays were fabricated on PDMS containing micro-ridge patterns and on superhydrophobic SU-8 pillar array. For the latter fabrication approach, DNA nanofiber with a diameter down to 40 nm could be fabricated. This approach would easily succeed in fabricating DNA nanofiber for the thermal transport study, especially to the scale

of 100 nm or less. The regular TET technique widely used to characterize the thermo-physical properties of micoscale wires and fibers was developed accordingly to address the issues associated with the experimental procedure. For the first time, a DNA nanofiber with a diameter of 150 nm was reported to have a thermal conductivity of 0.6 W/m·K.

6.2. Future work

Further studies on the thermal transport in DNA need to be conducted within nanoscale, from DNA bundle with a diameter of 100 nm or less to a single DNA molecule. Current work has shown the feasibilities to fabricate DNA nanofibers with a diameter down to 40 nm and to evaluate the thermo-physical properties of a DNA nanofiber with a diameter of 150 nm. However, a couple of issues in current experimental setup should be addressed. One major issue is the heat conduction to the air environment, which contributes a great ideal of thermal effects in the experiment. To exclude the air effect, the only option is to have the thermal characterization conducted in a high-vacuum chamber. This requires the abandon of probe station and thus the to-be-measured DNA nanofiber should be prepared between electrodes with large surface accessible for the ease of probing. As a result, this requires a complete change of the SU 8 pillar array design for DNA nanofiber fabrication. It is possible to fabricate DNA nanofiber array suspended between SU-8 pillars in which the pillar can be comparably very large. As long as the DNA solution stays on the pillars, DNA nanofibers could have the chance to be stretched between the large pillars. In addition, large electrode allows the application of silver paste to eliminate the electrical and thermal contact resistances. Therefore, DNA nanofiber suspended over large electrodes is an essential to continue the thermal transport study in DNA down to nanoscale.

One more factor that could also have an impact on the thermal transport in DNA is the base sequences. For example, homogeneous DNA built with same base pair could be considered as single crystal, which is expected to possess a much higher thermal transport capacity than nonhomogeneous DNA. As a matter of fact, the base sequences of DNA can be designed and easily controlled. This highlights DNA as a terrific candidate to define its thermal transport capacity through defining its own structure, i.e. base sequences. This will empower DNA to be applied to different scenarios, facilitating heat dissipation or creating heat insulation. In addition, manipulation of base sequences will also enable the fundamental research on the mechanisms of thermal transport in DNA.

REFERENCES

(1) Mirkin, C. A.; Letsinger, R. L.; Mucic, R. C.; Storhoff, J. J., A DNA-based method for rationally assembling nanoparticles into macroscopic materials. *Nature* **1996,** *382(6592)*, 607-609.

(2) Alivisatos, A. P.; Johnsson, K. P.; Peng, X.; Wilson, T. E.; Loweth, C. J.; Bruchez, M. P.; Schultz, P. G., Organization of 'nanocrystal molecules' using DNA. *Nature* **1996,** *382(6592)*, 609-611.

(3) Braun, E.; Eichen, Y.; Sivan, U.; Ben-Yoseph, G., DNA-templated assembly and electrode attachment of a conducting silver wire. *Nature* **1998,** *391(6669)*, 775-778.

(4) Wang, X.; Liu, F.; Andavan, G. T. S.; Jing, X.; Singh, K.; Yazdanpanah, V. R.; Bruque, N.; Pandey, R. R.; Lake, R.; Ozkan, M.; Wang, K. L.; Ozkan, C. S., Carbon Nanotube–DNA Nanoarchitectures and Electronic Functionality. *Small* **2006,** *2(11)*, 1356-1365.

(5) Dekker, C.; Ratner, M. A., Electronic properties of DNA. *Physics World* **2001**, 29-33.

(6) Berlin, Y. A.; Burin, A. L.; Ratner, M. A., Charge Hopping in DNA. *Journal of the American Chemical Society* **2001,** *123(2)*, 260-268.

(7) Bixon, M.; Giese, B.; Wessely, S.; Langenbacher, T.; Michel-Beyerle, M. E.; Jortner, J., Long-range charge hopping in DNA. *Proceedings of the National Academy of Sciences* **1999,** *96(21)*, 11713-11716.

(8) Giese, B.; Amaudrut, J.; Kohler, A.-K.; Spormann, M.; Wessely, S., Direct observation of hole transfer through DNA by hopping between adenine bases and by tunnelling. *Nature* **2001,** *412(6844)*, 318-320.

(9) Cai, L.; Tabata, H.; Kawai, T., Self-assembled DNA networks and their electrical conductivity. *Applied Physics Letters* **2000,** *77(19)*, 3105-3106.

(10) de Pablo, P. J.; Moreno-Herrero, F.; Colchero, J.; Gómez Herrero, J.; Herrero, P.; Baró, A. M.; Ordejón, P.; Soler, J. M.; Artacho, E., Absence of dc-Conductivity in lambda-DNA. *Physical Review Letters* **2000,** *85(23)*, 4992-4995.

(11) Porath, D.; Bezryadin, A.; de Vries, S.; Dekker, C., Direct measurement of electrical transport through DNA molecules. *Nature* **2000,** *403(6770)*, 635-638.

(12) Storm, A. J.; van Noort, J.; de Vries, S.; Dekker, C., Insulating behavior for DNA molecules between nanoelectrodes at the 100 nm length scale. *Applied Physics Letters* **2001,** *79(23)*, 3881-3883.

(13) Zhang, Y.; Austin, R. H.; Kraeft, J.; Cox, E. C.; Ong, N. P., Insulating Behavior of lambda-DNA on the Micron Scale. *Physical Review Letters* **2002,** *89(19)*, 198102.

(14) Fink, H.-W.; Schonenberger, C., Electrical conduction through DNA molecules. *Nature* **1999,** *398(6726)*, 407-410.

(15) Yoichi, O.; Hea-yeon, L.; Jian-hua, G.; Jeong, O. L.; Kyung-Hwa, Y.; Hidekazu, T.; Hitoshi, T.; Tomoji, K., Influence of Humidity on the Electrical Conductivity of Synthesized DNA Film on Nanogap Electrode. *Japanese Journal of Applied Physics* **2002,** *41(2R)*, 891-894.

(16) Kasumov, A. Y.; Kociak, M.; Guéron, S.; Reulet, B.; Volkov, V. T.; Klinov, D. V.; Bouchiat, H., Proximity-Induced Superconductivity in DNA. *Science* **2001,** *291(5502)*, 280-282.

(17) Velizhanin, K. A.; Chien, C.-C.; Dubi, Y.; Zwolak, M., Driving denaturation: Nanoscale thermal transport as a probe of DNA melting. *Physical Review E* **2011,** *83(5)*, 050906.

(18) Savin, A. V.; Mazo, M. A.; Kikot, I. P.; Manevitch, L. I.; Onufriev, A. V., Heat conductivity of the DNA double helix. *Physical Review B* **2011,** *83(24)*, 245406.

(19) Kodama, T.; Jain, A.; Goodson, K. E., Heat Conduction through a DNA−Gold Composite. *Nano Letters* **2009,** *9(5)*, 2005-2009.

(20) Chen, J.; Darst, S. A.; Thirumalai, D., Promoter melting triggered by bacterial RNA polymerase occurs in three steps. *Proceedings of the National Academy of Sciences* **2010,** *107(28)*, 12523-12528.

(21) Guan, J.; Boukany, P. E.; Hemminger, O.; Chiou, N.-R.; Zha, W.; Cavanaugh, M.; Lee, L. J., Large Laterally Ordered Nanochannel Arrays from DNA Combing and Imprinting. *Advanced Materials* **2010,** *22(36)*, 3997-4001.

(22) Harfenist, S. A.; Cambron, S. D.; Nelson, E. W.; Berry, S. M.; Isham, A. W.; Crain, M. M.; Walsh, K. M.; Keynton, R. S.; Cohn, R. W., Direct Drawing of Suspended Filamentary Micro- and Nanostructures from Liquid Polymers. *Nano Letters* **2004,** *4(10)*, 1931-1937.

(23) Perepelytsya, S. M.; Glibitskiy, G. M.; Volkov, S. N., Texture formation in DNA films with alkali metal chlorides. *Biopolymers* **2013,** *99(8)*, 508-516.

(24) Ushigome, T.; Shikazono, N.; Fujii, K.; Watanabe, R.; Suzuki, M.; Tsuruoka, C.; Tauchi, H.; Yokoya, A., Yield of Single- and Double-Strand Breaks and Nucleobase Lesions in Fully Hydrated Plasmid DNA Films Irradiated with High-LET Charged Particles. *Radiation Research* **2012,** *177(5)*, 614-627.

(25) Guo, J.; Wang, X.; Wang, T., Thermal characterization of microscale conductive and nonconductive wires using transient electrothermal technique. *Journal of Applied Physics* **2007,** *101(6)*, 063537.

(26) Guo, J.; Wang, X.; Zhang, L.; Wang, T., Transient thermal characterization of micro/submicroscale polyacrylonitrile wires. *Applied Physics A* **2007,** *89(1)*, 153-156.

(27) Guo, L.; Wang, J.; Lin, Z.; Gacek, S.; Wang, X., Anisotropic thermal transport in highly ordered TiO2 nanotube arrays. *Journal of Applied Physics* **2009,** *106(12)*, 123526.

(28) Feng, X.; Wang, X., Thermophysical properties of free-standing micrometer-thick Poly(3-hexylthiophene) films. *Thin Solid Films* **2011,** *519(16)*, 5700-5705.

(29) Feng, X.; Wang, X.; Chen, X.; Yue, Y., Thermo-physical properties of thin films composed of anatase TiO2 nanofibers. *Acta Materialia* **2011,** *59(5)*, 1934-1944.

(30) Huang, X.; Wang, J.; Eres, G.; Wang, X., Thermophysical properties of multi-wall carbon nanotube bundles at elevated temperatures up to 830 K. *Carbon* **2011,** *49(5)*, 1680-1691.

(31) Feng, X.; Huang, X.; Wang, X., Nonlinear effects in transient electrothermal characterization of anatase TiO2 nanowires. *Review of Scientific Instruments* **2012,** *83(4)*, 044901.

(32) Liu, G.; Huang, X.; Wang, Y.; Zhang, Y.-Q.; Wang, X., Thermal transport in single silkworm silks and the behavior under stretching. *Soft Matter* **2012,** *8(38)*, 9792-9799.

(33) Feng, X.; Huang, X.; Wang, X., Thermal conductivity and secondary porosity of single anatase TiO 2 nanowire. *Nanotechnology* **2012,** *23(18)*, 185701.

(34) Feng, X.; Liu, G.; Xu, S.; Lin, H.; Wang, X., 3-dimensional anisotropic thermal transport in microscale poly(3-hexylthiophene) thin films. *Polymer* **2013,** *54(7)*, 1887-1895.

(35) Van Velson, N.; Wang, X., Characterization of thermal transport across single-point contact between micro-wires. *Applied Physics A* **2013,** *110(2)*, 403-412.

(36) Liu, G.; Xu, S.; Cao, T.-T.; Lin, H.; Tang, X.; Zhang, Y.-Q.; Wang, X., Thermally induced increase in energy transport capacity of silkworm silks. *Biopolymers* **2014,** *101(10)*, 1029-1037.

(37) Xu, Z.; Wang, X.; Xie, H., Promoted electron transport and sustained phonon transport by DNA down to 10 K. *Polymer* **2014,** *55(24)*, 6373-6380.

(38) Xu, Z.; Xu, S.; Tang, X.; Wang, X., Energy transport in crystalline DNA composites. *AIP Advances* **2014,** *4(1)*, 017131.

(39) Datta, A. K., Biological and bioenvironmental heat and mass transfer. Marcel Dekker: New York, 2002.

(40) Kittel, C.,Introduction to solid state physics. 8th ed.; J. Wiley: Hoboken, NJ, 2005.

(41) Lin, H.; Xu, S.; Li, C.; Dong, H.; Wang, X., Thermal and electrical conduction in 6.4 nm thin gold films. *Nanoscale* **2013,** *5(11)*, 4652-4656.

(42) Wang, H.-D.; Liu, J.-H.; Zhang, X.; Guo, Z.-Y.; Takahashi, K., Experimental study on the influences of grain boundary scattering on the charge and heat transport in gold and platinum nanofilms. *Heat and Mass Transfer* **2011,** *47(8)*, 893-898.

(43) Zhang, Q. G.; Cao, B. Y.; Zhang, X.; Fujii, M.; Takahashi, K., Influence of grain boundary scattering on the electrical and thermal conductivities of polycrystalline gold nanofilms. *Physical Review B* **2006,** *74(13)*, 134109.

(44) Hu, H.; Wang, X.; Xu, X., Generalized theory of the photoacoustic effect in a multilayer material. *Journal of Applied Physics* **1999,** *86(7)*, 3953-3958.

(45) Wang, T.; Wang, X.; Zhang, Y.; Liu, L.; Xu, L.; Liu, Y.; Zhang, L.; Luo, Z.; Cen, K., Effect of zirconium(IV) propoxide concentration on the thermophysical properties of hybrid organic-inorganic films. *Journal of Applied Physics* **2008,** *104(1)*, 013528.

(46) Wang, X.; Zhong, Z.; Xu, J., Noncontact thermal characterization of multiwall carbon nanotubes. *Journal of Applied Physics* **2005,** *97(6)*, 064302.

(47) Xu, Y.; Zhang, Y.; Suhir, E.; Wang, X., Thermal properties of carbon nanotube array used for integrated circuit cooling. *Journal of Applied Physics* **2006,** *100(7)*, 074302.

(48) Wang, X.; Hu, H.; Xu, X., Photo-Acoustic Measurement of Thermal Conductivity of Thin Films and Bulk Materials. *Journal of Heat Transfer* **2000,** *123(1)*, 138-144.

(49) Downs, R. T.; Bartelmehs, K. L.; Gibbs, G. V.; Boisen, M. B., Interactive software for calculating and displaying X-ray or neutron powder diffractometer patterns of crystalline materials. *American Mineralogist* **1993,** *78(9-10)*, 1104-1107.

(50) Chemical Rubber Company.,Handbook of chemistry and physics. CRC Press: Cleveland, Ohio, 2004.

(51) Selbach, E.; Jacques, H.; Eiermann, K.; Lengeler, B.; Schilling, W., Electrical resistivity and lattice parameters of sputtered iridium alloys. *Thin Solid Films* **1987,** *149(1)*, 17-28.

(52) White, G. K.; Woods, S. B., Electrical and Thermal Resistivity of the Transition Elements at Low Temperatures. *Philosophical Transactions of the Royal Society of London. Series A, Mathematical and Physical Sciences* **1959,** *251(995)*, 273-302.

(53) Ma, W.; Zhang, X.; Takahashi, K., Electrical properties and reduced Debye temperature of polycrystalline thin gold films. *Journal of Physics D: Applied Physics* **2010,** *43(46)*, 465301.

(54) Chelikowsky, J. R.; Louie, S. G.,Quantum theory of real materials. Kluwer Academic Publishers: Boston, 1996.

(55) Katsnelson, M. I.; Naumov, I. I.; Trefilov, A. V.; Khlopkin, M. N.; Khromov, K. Y., Peculiarities of phonon spectra and lattice heat capacity in Ir aned Rh. *Philosophical Magazine Part B* **1997,** *75(3)*, 389-406.

(56) Bid, A.; Bora, A.; Raychaudhuri, A. K., Temperature dependence of the resistance of metallic nanowires of diameter >=15 nm: Applicability of Bloch-Grüneisen theorem. *Physical Review B* **2006,** *74(3)*, 035426.

(57) Kästle, G.; Boyen, H. G.; Schröder, A.; Plettl, A.; Ziemann, P., Size effect of the resistivity of thin epitaxial gold films. *Physical Review B* **2004,** *70(16)*, 165414.

(58) Zhang, W.; Brongersma, S. H.; Li, Z.; Li, D.; Richard, O.; Maex, K., Analysis of the size effect in electroplated fine copper wires and a realistic assessment to model copper resistivity. *Journal of Applied Physics* **2007,** *101(6)*, 063703.

(59) Powell, R. W.; Tye, R. P.; Woodman, M. J., The thermal conductivity and electrical resistivity of polycrystalline metals of the platinum group and of single crystals of ruthenium. *Journal of the Less Common Metals* **1967,** *12(1)*, 1-10.

(60) Powell, R. W.; Tye, R. P.; Woodman, M. J., Electrical Resistivities of the Platinum Metals. *Platinum Metals Review* **1962,** *6(4)*, 138-143.

(61) Chang, S.-S.; Westrum, E. F.; Carlson, H. G., Heat Capacities of Polyethylene III. One Linear and One Branched Sample from 5 to 350 K. *Journal of Research of the National Bureau of Standards Section a-Physics and Chemistry* **1975,** *79A(2)*, 437-441.

(62) Mrevlishvili, G. M., Low-temperature heat capacity of biomacromolecules and the entropic cost of bound water in proteins and nucleic acids (DNA). *Thermochimica Acta* **1998,** *308(1–2)*, 49-54.

(63) Purdue University. Thermophysical Properties Research Center.; Touloukian, Y. S.,Thermophysical properties of matter; the TPRC data series. IFI/Plenum: New York, 1970.

(64) Śmiałek, M. A.; Jones, N. C.; Hoffmann, S. V.; Mason, N. J., Measuring the density of DNA films using ultraviolet-visible interferometry. *Physical Review E* **2013,** *87(6)*, 060701.

(65) Maret, G.; Oldenbourg, R.; Winterling, G.; Dransfeld, K.; Rupprecht, A., Velocity of High-Frequency Sound-Waves in Oriented DNA Fibers and Films Determined by Brillouin-Scattering. *Colloid and Polymer Science* **1979,** *257(10)*, 1017-1020.

(66) Gu, Q.; Cheng, C.; Gonela, R.; Suryanarayanan, S.; Anabathula, S.; Dai, K.; Haynie, D. T., DNA nanowire fabrication. *Nanotechnology* **2006,** *17(1)*, R14.

(67) Lin, H.; Xu, S.; Li, C.; Dong, H.; Wang, X. W., Thermal and electrical conduction in 6.4 nm thin gold films. *Nanoscale* **2013,** *5(11)*, 4652-4656.

(68) Cook, J. G.; Meer, M. P. v. d., The thermal conductivity and electrical resistivity of gold from 80 to 340 K. *Canadian Journal of Physics* **1970,** *48(3)*, 254-263.

(69) Damon, D. H.; Mathur, M. P.; Klemens, P. G., Phonon-Assisted Impurity Scattering in Gold Alloys. *Physical Review* **1968,** *176(3)*, 876-885.

(70) Ashcroft, N. W.; Mermin, N. D.,Solid state physics. Holt: New York, 1976.

(71) Davidson, N.; Szybalski, W.,Chapter 3 Physical and Chemical Characteristics of Lambda DNA. Cold Spring Harbor Monograph Archive: 1971.

(72) Broerman, A. W.; Venerus, D. C.; Schieber, J. D., Evidence for the stress-thermal rule in an elastomer subjected to simple elongation. *The Journal of Chemical Physics* **1999,** *111(15)*, 6965-6969.

(73) van den Brule, B. H. A. A., A network theory for the thermal conductivity of an amorphous polymeric material. *Rheologica Acta* **1989,** *28(4)*, 257-266.

(74) Venerus, D. C.; Schieber, J. D.; Iddir, H.; Guzmán, J.; Broerman, A., Anisotropic Thermal Diffusivity Measurements in Deforming Polymers and the Stress-Thermal Rule. *International Journal of Thermophysics* **2001,** *22(4)*, 1215-1225.

(75) Bensimon, A.; Simon, A.; Chiffaudel, A.; Croquette, V.; Heslot, F.; Bensimon, D., Alignment and Sensitive Detection of DNA by a Moving Interface. *Science* **1994,** *265(5181)*, 2096-2098.

(76) Bensimon, D.; Simon, A. J.; Croquette, V.; Bensimon, A., Stretching DNA with a Receding Meniscus - Experiments and Models. *Physical Review Letters* **1995,** *74(23)*, 4754-4757.

(77) Allemand, J. F.; Bensimon, D.; Jullien, L.; Bensimon, A.; Croquette, V., pH-dependent specific binding and combing of DNA. *Biophysical Journal* **1997,** *73(4)*, 2064-2070.

(78) Yokota, H.; Johnson, F.; Lu, H. B.; Robinson, R. M.; Belu, A. M.; Garrison, M. D.; Ratner, B. D.; Trask, B. J.; Miller, D. L., A new method for straightening DNA molecules for optical restriction mapping. *Nucleic Acids Research* **1997,** *25(5)*, 1064-1070.

(79) Michalet, X.; Ekong, R.; Fougerousse, F.; Rousseaux, S.; Schurra, C.; Hornigold, N.; vanSlegtenhorst, M.; Wolfe, J.; Povey, S.; Beckmann, J. S.; Bensimon, A., Dynamic molecular combing: Stretching the whole human genome for high-resolution studies. *Science* **1997,** *277(5331)*, 1518-1523.

(80) Gueroui, Z.; Place, C.; Freyssingeas, E.; Berge, B., Observation by fluorescence microscopy of transcription on single combed DNA. *Proceedings of the National Academy of Sciences of the United States of America* **2002,** *99(9)*, 6005-6010.

(81) Otobe, K.; Ohtani, T., Behavior of DNA fibers stretched by precise meniscus motion control. *Nucleic Acids Research* **2001,** *29(22)*, e109.

(82) Guan, J.; Lee, L. J., Generating highly ordered DNA nanostrand arrays. *Proceedings of the National Academy of Sciences of the United States of America* **2005,** *102(51)*, 18321-18325.

(83) Guan, J.; Ferrell, N.; Yu, B.; Hansford, D. J.; Lee, L. J., Simultaneous fabrication of hybrid arrays of nanowires and micro/nanoparticles by dewetting on micropillars. *Soft Matter* **2007,** *3(11)*, 1369-1371.

(84) Guan, J.; Yu, B.; Lee, L. J., Forming Highly Ordered Arrays of Functionalized Polymer Nanowires by Dewetting on Micropillars. *Advanced Materials* **2007,** *19(9)*, 1212-1217.

(85) Cheng, J.-J.; Chang, Y.-H.; Huang, W.-Y.; Juang, Y.-J., Effect of solution viscosity on generating long DNA nanostrands array via patterned molecular combing. *Applied Physics Letters* **2009,** *94(24)*, 244101.

(86) Lin, C. H.; Guan, J.; Chau, S. W.; Lee, L. J., Experimental and numerical analysis of DNA nanostrand array formation by molecular combing on microwell-patterned surface. *Journal of Physics D: Applied Physics* **2009,** *42(2)*, 025303.

(87) Miele, E.; Accardo, A.; Falqui, A.; Marini, M.; Giugni, A.; Leoncini, M.; De Angelis, F.; Krahne, R.; Di Fabrizio, E., Writing and Functionalisation of Suspended DNA Nanowires on Superhydrophobic Pillar Arrays. *Small* **2015,** *11(1)*, 134-140.

(88) Gentile, F.; Coluccio, M. L.; Limongi, T.; Perozziello, G.; Candeloro, P.; Di Fabrizio, E., The Five Ws (and one H) of Super-Hydrophobic Surfaces in Medicine. *Micromachines* **2014,** *5(2)*, 239-262.

(89) Shirtcliffe, N. J.; McHale, G.; Atherton, S.; Newton, M. I., An introduction to superhydrophobicity. *Advances in Colloid and Interface Science* **2010,** *161(1-2)*, 124-138.

(90) Milne, A. J. B.; Amirfazli, A., The Cassie equation: How it is meant to be used. *Advances in Colloid and Interface Science* **2012,** *170(1-2)*, 48-55.

(91) Marquez-Velasco, J.; Vlachopoulou, M. E.; Tserepi, A.; Gogolides, E., Stable superhydrophobic surfaces induced by dual-scale topography on SU-8. *Microelectronic Engineering* **2010,** *87(5-8)*, 782-785.

(92) Gentile, F.; Moretti, M.; Limongi, T.; Falqui, A.; Bertoni, G.; Scarpellini, A.; Santoriello, S.; Maragliano, L.; Zaccaria, R. P.; di Fabrizio, E., Direct Imaging of DNA Fibers: The Visage of Double Helix. *Nano Letters* **2012,** *12(12)*, 6453-6458.

(93) De Angelis, F.; Gentile, F.; Mecarini, F.; Das, G.; Moretti, M.; Candeloro, P.; Coluccio, M. L.; Cojoc, G.; Accardo, A.; Liberale, C.; Zaccaria, R. P.; Perozziello, G.; Tirinato, L.; Toma, A.; Cuda, G.; Cingolani, R.; Di Fabrizio, E., Breaking the diffusion limit with super-hydrophobic delivery of molecules to plasmonic nanofocusing SERS structures. *Nature Photonics* **2011,** *5(11)*, 683-688.

(94) Ciasca, G.; Businaro, L.; Papi, M.; Notargiacomo, A.; Chiarpotto, M.; Ninno, A. D.; Palmieri, V.; Carta, S.; Giovine, E.; Gerardino, A.; Spirito, M. D., Self-assembling of large ordered DNA arrays using superhydrophobic patterned surfaces. *Nanotechnology* **2013,** *24(49)*, 495302.

(95) Su, B.; Wang, S. T.; Wu, Y. C.; Chen, X.; Song, Y. L.; Jiang, L., Small Molecular Nanowire Arrays Assisted by Superhydrophobic Pillar-Structured Surfaces with High Adhesion. *Advanced Materials* **2012,** *24(20)*, 2780-2785.

(96) Klein, H. H.; Karni, J.; Ben-Zvi, R.; Bertocchi, R., Heat transfer in a directly irradiated solar receiver/reactor for solid–gas reactions. *Solar Energy* **2007,** *81(10)*, 1227-1239.

(97) Wang, H.-D.; Liu, J.-H.; Guo, Z.-Y.; Zhang, X.; Zhang, R.-F.; Wei, F.; Li, T.-Y., Thermal Transport Across the Interface Between a Suspended Single-Walled Carbon

Nanotube and Air. *Nanoscale and Microscale Thermophysical Engineering* **2013,** *17(4)*, 349-365.

(98) Chalabi, H.; Buchina, O.; Saraceno, L.; Lorenzini, M.; Valougeorgis, D.; Morini, G. L., Experimental analysis of heat transfer between a heated wire and a rarefied gas in an annular gap with high diameter ratio. *Journal of Physics: Conference Series* **2012,** *362(1)*, 012028.